CO_2-Foams for Enhanced Oil Recovery and CO_2 Storage

Arthur Uno Rognmo

Dissertation for the Degree of Philosophiae Doctor (PhD)
University of Bergen, Norway
2019

UNIVERSITY OF BERGEN

CO_2-Foams for Enhanced Oil Recovery and CO_2 Storage

Arthur Uno Rognmo

Dissertation for the Degree of Philosophiae Doctor (PhD)

at the University of Bergen

2019

Date of defense: 01.03.2019

Year: 2019

Title: CO_2-Foams for Enhanced Oil Recovery and CO_2 Storage

Name: Arthur Uno Rognmo

Print: Skipnes Kommunikasjon / University of Bergen

“As far as the laws of mathematics refer to reality, they are not certain; and as far as they are certain, they do not refer to reality.”

- Albert Einstein

Acknowledgements

This dissertation is the result of several years of hard work and late nights in front of textbooks, the computer and at the laboratory. I have received invaluable support along the way and I would like to take this opportunity to thank these people.

I want to acknowledge the Research Council of Norway for financial support through the CLIMIT program, Nouryon, Shell, Total and Equinor for project support and guidance. A special thanks to Andreas Sundblom (Nouryon) for all help and insight.

I would like to thank my supervisors Prof. Martin A. Fernø and Prof. Arne Graue at the Department of Physics and Technology, University of Bergen. I have greatly appreciated the opportunity to work on inspiring projects over these last couple of years.

I want to thank the students and staff associated with the Reservoir Physics Group, as well as my fellow colleagues for contributing to a good learning environment and being willing to share their experience and knowledge.

Vegard Gjerde and Dr. Kristoffer Johansen deserve gratitude for being good conversationalists and providing valuable motivational input. Thanks to the mechanical workshop for outstanding craftsmanship and Villy Nielsen for making sure that every day of work started off with a big smile.

I want to express my deepest appreciation to my parents for their unconditional love and for encouraging me to reach my full potential by teaching me the value of hard work and integrity.

My girlfriend, Jeanette Hamrane Angen, thank you for being an amazing source of inspiration, motivation and support.

Bergen, November 2018

Arthur Uno Rognmo

Summary

Human prosperity, economic growth and energy supply have shown a strong positive correlation from the start of the industrial revolution until the present. During the 20th century, cheap and reliable energy from fossil sources became abundantly available. Concerns regarding climate change, however, are increasingly problematized by contemporary scientists and policymakers. In particular, the emission of carbon dioxide (CO_2) is considered an important issue to solve, as it is the main contributor to the greenhouse effect. Reducing CO_2 emissions, while providing the world with cheap, plentiful and reliable energy will therefore be vital for a prosperous future.

Atmospheric CO_2 accumulation can be mitigated by capturing CO_2 and storing it in suitable underground formations. Large-scale implementation of carbon capture and storage (CCS) can contribute to stabilize atmospheric greenhouse gas concentrations. For profit maximizing companies, implementation costs related to CCS are high compared to that associated with atmospheric release. Economic incentives can be significantly increased by using CO_2 as an input parameter in a production process, thereby adding value to the end product. One alternative is to use anthropogenic CO_2 for enhanced oil recovery (EOR), which promotes investments into safe CO_2 storage while improving the oil production process. This synergy is likely to accelerate technological advances related to CO_2 storage and reduce lifecycle emissions from the oil production projects.

At reservoir conditions, CO_2 has several advantageous characteristics for EOR purposes. For this reason, it has been implemented as an oil displacement agent for more than 50 years. Pure CO_2 injection, however, has some inherent challenges due to density and viscosity differences between reservoir fluids and CO_2. The former discrepancy causes CO_2 to migrate towards the top of the reservoir, while the latter discrepancy promotes formation of viscous fingers and gas channeling through high permeable zones. Both effects are detrimental to oil recovery and CO_2 storage, since unstable displacement fronts decrease sweep efficiency and reduce storage.

Consequently, project profitability will be adversely affected through lower oil recovery.

Reducing CO_2 mobility is important to mitigate flow instabilities. *In-situ* foam generation is one possible solution, where a mixture of CO_2 and brine with a foaming agent (surfactants or nanoparticles) has proven to significantly reduce CO_2 mobility and front propagation. Foams are inherently thermodynamically unstable, but this aspect can be improved by optimizing type and concentration of the foaming agent. Surfactants have shown to generate strong foams through laboratory experiments (and partly in field trials), but might destabilize at tough reservoir conditions such as high temperatures and salinities. Nanoparticles are currently being evaluated as a foam agent and several laboratory results show great promise. High adhesive energies on interfaces, low cost and ability to remain stable in harsh environments are all properties advocating for further research. Compared to surfactants, nanoparticles as foaming agents for EOR is a novel technology and has as of yet not been tested in fields.

This dissertation is part of two larger research projects on CO_2-foam applications for storage and enhanced oil recovery: «Nanoparticles to Stabilize CO_2-foam for Efficient CCUS in Challenging Reservoirs» (the Research Council of Norway project number 268216) and «CO_2 Storage from Lab to On-Shore Field Pilots Using CO_2-Foam for Mobility Control in CCUS» (the Research Council of Norway project number 249742). By implementing a bottom-up scientific approach, foam systems in sandstones and carbonates have been evaluated and optimized for EOR and CO_2 storage performance.

This dissertation consists of two parts. The first part contains the introduction, theoretical background and a review of key findings. It is intended to corroborate and summarize the six scientific papers listed in the second part. The main objective of this work is to provide new insight into CO_2-foam behavior in porous media and optimize foam performance for field application. Adapting an experimental approach, two areas of focus are prioritized: i) delineating causal relationships between concepts and principles related to CO_2-foam behavior in porous media; and ii) providing input to a field-scale simulation model to optimize foam performance in field trial.

Paper 1 demonstrates the broad applicability of CO_2 injection in a CCUS context. Ultra-low permeabilities associated with shale oil formations exclude conventional waterflooding for EOR. Supercritical CO_2 enabled flow through the matrix core plugs, resulting in (enhanced) oil production and associated CO_2 storage. Observations indicated adverse effects from pure CO_2 injection, including low sweep efficiency, early CO_2 breakthrough and low oil recovery.

Paper 2 implements a bottom-up multi-scale approach to evaluate surfactant-stabilized CO_2-foams with a preselected field specific nonionic surfactant. Observations indicated strong foam generation with resulting flow diversion from co-injection of CO_2 and surfactant solution on pore-scale. Increased thermodynamic stability was quantified during static, no-flow, tests over several days. Input parameters for a commercial foam simulation model were obtained from CO_2 and CO_2-foam injections in reservoir core plugs (end-point relative permeabilities, maximum mobility reduction factor and viscoelastic properties). The laboratory data suggested an optimal volumetric gas fraction between 0.60 and 0.70. EOR and CO_2 storage were evaluated at reservoir conditions, showing higher CO_2 storage and increased oil recovery during foam injections in presence of oil. Results indicated a carbon neutral oil production from CO_2-foam injection, where 96% of the carbon atoms in the produced oil was stored (as CO_2) in an *ax-ante* storage process.

Paper 3 extends on the bottom-up approach from Paper 2 and evaluates CO_2-foam performance in reservoir core plugs with reservoir fluids. Surfactant concentration (0.5 wt%), injection strategy (multi-cycle SAG) and slug sizes (macroscopic average gas fraction of 70%) were determined for field injection, based on experimental data and simulations.

Paper 4 evaluated nanoparticles as possible foam stabilizers for CO_2-foams in sandstones. Loss to the formation (retention) and stability during nanofluid flow through porous media were measured at 20ºC, with no observed decrease in flow potential. The ability of nanoparticles to stabilize CO_2-foams was determined by comparing co-injections of nanofluid and CO_2 to baseline co-injections (CO_2 and brine

without foaming agent). Foam generation and stabilization effects were observed through higher apparent viscosities. Results showed increased apparent viscosities from surfactant-stabilized foams (compared to nanoparticle-stabilized foams) administered at the same experimental conditions. Injection history and gas saturation indicated strong hysteretic effects during foam scans.

Paper 5 extends on Paper 4 to investigate CO_2-foam performance with two different nanoparticles and a surfactant in presence of crude oil. The temperature was increased from 20ºC to 60ºC, while the other experimental conditions remained constant. Emphasis was put on increasing statistical significance of reported data by performing several injection tests at identical conditions. Results showed that nanoparticles have a higher stabilizing effect on CO_2-foams compared to surfactants, implying more resistance to destabilization from crude oil. Incremental oil recoveries, however, are similar for surfactant and nanoparticle-stabilized CO_2-foams, suggesting different EOR mechanisms governing the displacement processes.

Paper 6 examines the ability of nanoparticles to stabilize CO_2-foams at tough reservoir conditions, such as increased temperatures, brine salinities and ionic strengths. The CO_2 storage potential was quantified during foam injections in core plugs, and a parameter for calculating CO_2 utilization was implemented. Nanoparticle-stabilized foams increased oil production and CO_2 storage potential by displacing more oil and water during tertiary EOR compared to baseline injections.

List of Publications

1. **Rognmo, A. U.**, Fredriksen, S. B., and Fernø, M. A. Unlocking the Potential without Fracking – CO_2 Injection in Tight Shale Oil. Reviewed Proceedings at *the International Symposium of the Society of Core Analysts*, Vienna, Austria. August, 2017. Featured in *Washington Post Opinions Column*, April, 2018.

2. **Rognmo, A. U.**, Fredriksen, S. B., Alcorn, Z. P., Fernø, M. A., and Graue, A. Pore-to-Core EOR Upscaling for CO_2-Foam for CCUS. Proceedings at *the SPE Europec featured at the 80th EAGE Annual Conference & Exhibition*, Copenhagen, Denmark. June, 2018. Paper: SPE-190869-MS. Revised and submitted to *SPE Journal,* October 2018.

3. Alcorn, Z. P., Fredriksen, S. B., Sharma, M., **Rognmo, A. U.,** Fernø, M.A., and Graue, A. An Integrated CO_2 Foam EOR Pilot Program with Combined CCUS in an Onshore Texas Heterogeneous Carbonate Field. Proceedings at *the SPE Improved Oil Recovery Conference,* Tulsa, OK, USA. April, 2018. Paper: SPE-190204-MS. Accepted for publication in *SPE Reservoir Evaluation and Engineering*, November 2018.

4. **Rognmo, A. U.**, Horjen, H., and Fernø, M. A. Nanotechnology for Improved CO_2 Utilization in CCS: Laboratory Study of CO_2-Foam Flow and Silica Nanoparticle Retention in Porous Media. *International Journal of Greenhouse Gas Control*. 2017.

5. **Rognmo, A. U.,** Heldal, S., and Fernø, M.A. Silica Nanoparticles to Stabilize CO_2-foam for Improved CO_2 Utilization: Enhanced CO_2 Storage and Oil Recovery from Mature Oil Reservoirs. *Fuel*. 2017.

6. **Rognmo, A. U.,** Al-Khayyat, N., Heldal, S., Vikingstad, I., Eide, Ø., Fredriksen, S. B., Alcorn, Z.P., Graue, A., Bryant, S. L., Kovscek, A. R., and Fernø, M. A. Performance of Silica Nanoparticles in CO_2-Foam for EOR and CCUS at Tough Reservoir Conditions. Proceedings at *the SPE Norway One Day Seminar*, Bergen, Norway. April, 2018. Paper: SPE-191318-MS. Revised and submitted to *SPE Journal,* September 2018.

Additional Publications

- Eide, Ø., Føyen, T., Skjelsvik, E., **Rognmo, A. U.,** and M.A. Fernø. Nanoparticle Stabilized Foam in Harsh Conditions for CO_2 EOR. Proceedings at *the Abu Dhabi International Petroleum Exhibition & Conference*, Abu Dhabi, UAE. November, 2018. Paper: SPE-193212-MS.

- Alcorn, Z. P., Sharma, M., Fredriksen, S. B., **Rognmo, A. U.**, Fernø, M. A., and Graue, A. CO_2 Foam Field Pilot Test for EOR and CO_2 Storage in a Heterogeneous Carbonate Reservoir: Operational Design, Data Collection and Pilot Monitoring Program. Extended Abstract at *EAGE 80th Annual Conference and Exhibition*, Copenhagen, Denmark. June, 2018.

- Fredriksen, S. B., **Rognmo, A. U.**, Sandengen, K., and Fernø, M. A. Wettability Effects on Osmosis as an Oil Mobilization Mechanism during Low-Salinity Waterflooding, *Petrophysics.* 2017.

- Fredriksen, S. B., **Rognmo, A. U.,** and Fernø, M. A., 2017. Pore-Scale Mechanisms during Low Salinity Waterflooding: Oil Mobilization by Diffusion and Osmosis, *Journal of Petroleum Science and Engineering*. 2018.

- Fernø, M. A., Hauge, L. P., **Rognmo, A. U.**, Gauteplass, J., and Graue, A. Flow visualization of CO_2 in tight shale formations at reservoir conditions, *Geophysical Research Letters*. 2015.

- Fredriksen, S. B., Alcorn, Z. P., Frøland, A., Viken, A., **Rognmo, A. U.,** Seland, J. G., Ersland, G., Fernø, M. A., and Graue, A., 2018. Surfactant Pre-Floods during CO_2 Foam for Integrated Enhanced Oil Recovery in Fractured Oil-Wet Carbonates. Proceedings at *the SPE IOR Symposium*, April, 2018. Tulsa, OK, USA. Paper: SPE-190168-MS. Accepted for publication in *SPE Journal*, November 2018.

Presentations at International Conferences

Pore-to-Core EOR Upscaling for CO_2-Foam for CCUS. Oral presentation at *the SPE Europec featured at the 80th EAGE Annual Conference & Exhibition*, Copenhagen, Denmark. June, 2018. Paper: SPE-190869-MS.

Performance of Silica Nanoparticles in CO_2-foam for EOR and CCUS at Tough Reservoir Conditions. Oral presentation at *the SPE Norway One Day Seminar,* Bergen, Norway. April, 2018. Paper: SPE-191318-MS.

Nanotechnology for increased CO_2 utilization: Laboratory study of Enhanced CO_2 Storage and Oil Recovery by CO_2-foam injection. Oral presentation at *the 3rd Biennial CO_2 for EOR as CCUS Conference,* Houston, TX, USA. October, 2017.

Unlocking the Potential without Fracking – CO_2 Injection in Tight Shale Oil. Oral presentation at *the International Symposium of the Society of Core Analysts*, Vienna, Austria. August, 2017.

CO_2 Injection for EOR in Tight Shales. Poster presentation at *the IOR Norway 2016 Conference*, Stavanger, Norway. April, 2016.

Contents

1. Introduction and Concepts

In this chapter, the motivation behind the dissertation, the theoretical background with special emphasis on relevant concepts and a description of the pilot project are given.

1.1 Energy Demand and Climate Change

Energy is an enabler of life and, alongside food and clean water, the provision of cheap, reliable and sustainable energy for future generations is a major global challenge. Renewable energy production is steadily increasing and the reliance on fossil fuels is expected to decrease from 86% in 2017 to 77% of the energy mix in 2040 [1]. However, the International Energy Agency projects an increase in the world energy consumption of 28% in total from 2015 to 2040 (reference case). In the same period, it is expected that the economic growth, measured by gross domestic product, will rise by 3.0% per year and remain a key determinant for energy demand. In addition to exploring new energy resources, therefore, the environmental impact from existing ones, e.g. the production of oil and gas, must be reduced to meet the United Nations Sustainable Development Goals [2].

The Intergovernmental Panel on Climate Change (IPCC) has concluded in their *Synthesis Report on Climate Change* (2014), that it is extremely likely that anthropogenic drivers are the dominant cause of the observed warming effect since the 1950s [3]. Anthropogenic greenhouse gas (GHG) emissions are at a record high and CO_2 is the most important anthropogenic GHG, contributing to ocean acidification, a rising sea level and overall higher temperatures. Failure to implement new technologies at an early stage will cause additional amounts of CO_2 to be released into the atmosphere and increase its negative impact.

1.2 Carbon Capture, Utilization and Storage

Carbon (dioxide) capture and storage (CCS) refers to the process of capturing anthropogenic CO_2 at large point sources and injecting it into subsurface formations

for secure long term storage [4]. The IPCC appoints CCS as one of several technologies that are essential to the mix of climate mitigation strategies to limit the increase in global mean temperature. Currently, low carbon price (cost of emitting CO_2) impedes large-scale investments for CCS implementation. This in turn reduces the rate of technological improvement. Some view CO_2-EOR as a possible solution to induce industry interest in CO_2 storage [5]. By using CO_2 as input in an oil production process, CO_2 is stored in the reservoir after the oil displacement. Additional costs associated with CO_2 injection are justified on two levels: i) financially, additional revenue is generated from the additional oil recovery; and ii) sustainability, reducing negative externalities from energy production. This process is referred to as carbon capture, utilization and storage (CCUS). By injecting CO_2 from anthropogenic sources, *ex-ante* storage reduces emissions from oil consumption which leads to a more sustainable energy production [6].

1.3 CO_2 Injection for EOR

The injection of pressurized CO_2 for enhanced oil recovery (EOR) has been implemented for decades [7-10] and combines pressure support with effective oil displacement. Residual oil is mobilized through oil swelling and viscosity reduction that result from interfacial tension (IFT) reduction between CO_2 and oil [9]. In locations where CO_2 is available for injection, as in the US Permian Basin, CO_2 is a cost-effective EOR injection fluid [11, 12]. Estimates from the "2014 worldwide EOR survey" suggest that 38% of EOR production in the US comes from CO_2 injection [13, 14]. Laboratory evaluations of CO_2 injection for EOR at miscible conditions demonstrate oil recoveries over 90% of original oil in place (OOIP) [15], whereas field-scale recoveries range from 10% to 20% of OOIP [16-18]. Front instabilities causing viscous fingering, gravitational segregation and gas flow in high permeable (thief) zones are the main reasons for the large discrepancy between laboratory and field observations. CO_2 injections thus experience early CO_2 breakthrough, poor sweep and high gas-oil production ratios (GOR), all of which are detrimental for oil recovery efficiency, CO_2 utilization and increase costs associated with CO_2 handling and re-injection. These

adverse effects are attributed to the density and viscosity of CO_2 (Figure 1) compared with those of the *in-situ* fluids (oil and water). Suggested mitigations include foam mobility control [19], conformance improvements [20], water alternating gas (WAG) [21] and CO_2 thickeners [22, 23]. This dissertation focuses on advancing *in-situ* generated CO_2-foam systems that contribute to in-depth mobility control.

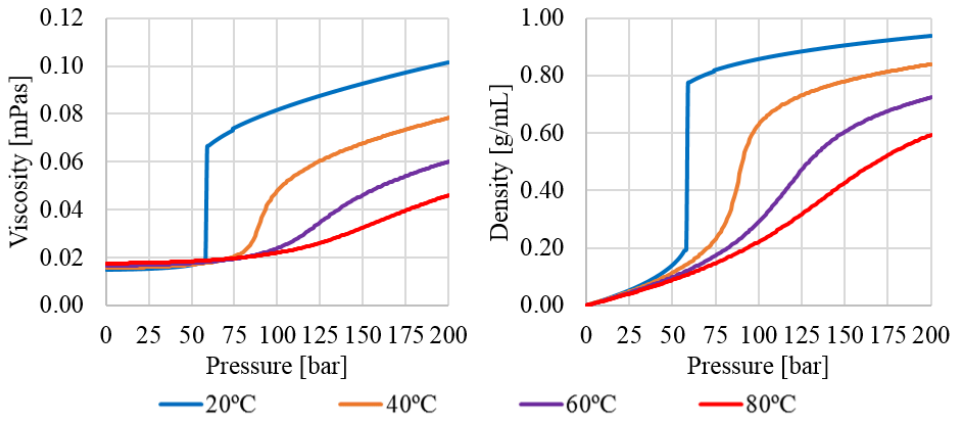

Figure 1: Density and viscosity of CO_2 as a function of pressure. Critical temperature and pressure: ~ 31ºC and ~74 bar (7.4 MPa) [24].

1.4 CO_2-Foam for EOR

Foams are defined as gas dispersed in a continuous liquid phase and have a wide range of applications [25, 26]. In everyday life, foams can be found in anything from shaving creams and soda heads to fire extinguishers. Their appearance in the petroleum industry ranges from use in well applications and oil refining processes to mobility control [25]. An illustration of an idealized two-phase foam system of liquid and gas is given in Figure 2. The gas phase is contained inside the liquid phase in multiple bubbles and separated by thin liquid films referred to as *lamellae*. This configuration can be achieved by flowing gas through the liquid phase or agitating a container with both phases present. In bulk, a two-phase system between water and a gas with this configuration would quickly be subject to foam coalescence and the foam structure would cease to exist. Increased thermodynamic stability of the foams can be achieved

by adding surface active agents (surfactants) or nanoparticles to the aqueous phase [25, 27-31] or to the CO_2 [32].

In porous media, foams can decrease the mobility of gas with several orders of magnitude [33, 34], mitigating front instabilities and diverting flow into un-swept regions of the reservoir [35]. Total mobility reduction is a combination of resistance to flow from moving and stationary lamellae. This is correlated to porous media properties such as pressure gradient, capillary pressure, saturation, pore geometry and bubble sizes [34, 36]. Stationary lamella affects relative permeability of gas by reducing mobile gas saturation and diverting gas flow paths [34, 36]. Mobile lamella are on the other hand retarded due to interaction with the pore walls [37].

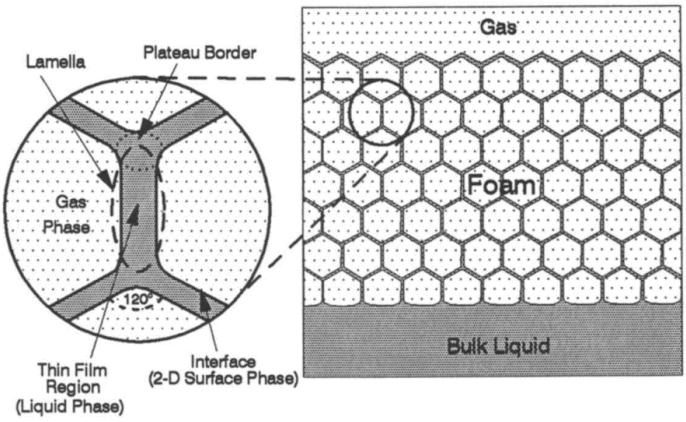

Figure 2: Generalized bulk foam system [38].

The use of CO_2-foam is a field tested technique proven to mitigate low sweep efficiencies. Examples of CO_2-foam field pilots with surfactant-stabilized foam are reported as technical successes (evidence of foam creation, improved sweep and enhanced oil recovery) in the literature [39-44], but full-field implementation was uneconomical. As of yet, no field pilots have been reported where nanoparticles are used as the foaming agent for CCS, CCUS or EOR purposes.

1.4.1 Foaming Agents

This dissertation focuses on the use of surfactants and nanoparticles, referred to as *foaming agents*, to increase foam stability and generation in porous media.

Surfactants

Surfactants are often used to improve generation and stabilize foams in porous media [19]. Due to their amphiphilic structure (both hydro- and lipophilic), they adsorb to the gas-liquid interface and decrease IFT [45]. There are four major classes of surfactants categorized by head group polarity: cationic, anionic, nonionic and zwitterionic [46]. The majority of work presented in this dissertation uses a commercially available nonionic surfactant (Huntsman International LLC, CAS no. 68551-12-2), referred to as *SurfA*. It was selected for the field pilot injection based on criteria such as ability to generate foam, degree of adsorption to the rock surface, thermal stability and partitioning coefficient. More information can be found elsewhere [47, 48]. In CO_2-foam injections at room temperatures (Paper 5), a commercially available anionic alpha-olefin sulfonate (AOS) surfactant (C_{14-16}) was used. AOS surfactants show low adsorptions in sandstones [49-51] and have been used in CO_2-foam projects [19].

Nanoparticles

Nanoparticles have gained attention towards EOR applications in recent years and are routinely used in a wide range of other industry applications, such as in solar cells [52-55], imaging [56] and drug delivery [57]. They are defined as particles with a size ranging from 1-100 nm and intrinsic properties different from those found in the bulk of the material due to their high surface-to-volume ratio [58]. Even though the use of silica nanoparticles for stabilizing emulsions of CO_2-in-water was described by Dickson *et al.* (2004) as an alternative to surfactants, it was not suggested for EOR purposes at the time [29]. The mechanical and thermal stability of nanoparticles make them robust and preferred foaming agents for injection at reservoir conditions because they can resist high temperatures, pressures, shear and salinity [30]. High surface adsorption energies associated with nanoparticles at interfaces practically eliminate them from being desorbed [59], adding stability to CO_2-foams. Two nanoparticles with

different hydrophilicity were evaluated in this work, both produced and delivered by Nouryon.

1.4.2 Conceptual Principles and Equations

An improved understanding of complex systems relies on a framework of models and conceptual principles. Describing foam floods in porous media is a complex task, governed by effects from wettability, foaming agents, phase interactions, state variables, oil compositions and fluid saturations, to name a few. This section includes some of the basic principles (and associated equations) from petroleum engineering and physics that are deemed relevant to gain insight into the multi-phase fluid flow interpretation presented in this dissertation. It promotes understanding by capturing contributions of different variables from observed phenomena, but is by no means exhaustive. Understanding foam behavior in porous media is essential to determine injection parameters for optimal CO_2-foam performance in fields.

Foam generation and destruction

Foam strength is strongly correlated to bubble density (lamellae per unit volume), quantified through apparent viscosity [37, 60, 61]. The number of lamellae is given by the ratio of generating to destruction rate, determined by underlying mechanisms. During flow in porous media, visual investigations have identified three widely recognized mechanisms describing *in-situ* foam generation: snap-off, lamella division and leave-behind [34]. Mechanisms for foam destruction include: gravity drainage [38], capillary suction [62] and gas diffusion [36, 38]. A detailed description of foam generating and destruction mechanisms can be found elsewhere [63, 64].

Throughout this dissertation, foam performance has been evaluated with respect to foam texture, foam strength, oil recovery efficiency and CO_2 storage. Pore-scale experiments enable direct visual assessments of foam strength based on texture (bubble density). Core-scale foam floods use differential pressure measurements as a proxy for describing foam strength, interpreted as the ability to reduce CO_2 mobility by the formation of lamellae. Increased differential pressures therefore imply stronger foams [37, 60, 61]. Foam strengths are reported in terms of the mobility reduction factor (MRF) (Paper 3), apparent viscosity (μ_{app}) (Papers 2, 3, 4 and 6), or as ratio of pressure

gradient increase during foam to pressure gradient during no foam (Papers 5 and 6). Apparent viscosity is calculated based on Darcy's law:

$$\mu_{app} = \frac{k\nabla P}{(u_l + u_g)} \quad (1)$$

where k is the absolute permeability, ∇P is the pressure gradient over the core plug while u_l and u_g are the superficial velocities of liquid and gas, respectively [65]. MRF is a dimensionless parameter defined as the ratio of pressure-drop during foam flood, ΔP_{foam}, to pressure-drop during no-foam flood, $\Delta P_{no\text{-}foam}$ [66]. From Equation 1 the MRF is given as the ratio of apparent viscosities of foam and no-foam floods, given constant k:

$$MRF = \frac{\Delta P_{foam}}{\Delta P_{no-foam}} = \frac{\mu_{foam}}{\mu_{no-foam}} \quad (2)$$

where ΔP is the pressure-drop over the core.

Fluid mobility, λ, describes the ability of a fluid to flow in porous media and is defined as the ratio of effective permeability to phase viscosity:

$$\lambda = \frac{k_{eff}}{\mu} \quad (3)$$

where k_{eff} is the effective permeability of the fluid (a function of the saturation) and μ is the viscosity of the fluid (a fluid property). From Equation 3 it is evident that the mobility of a fluid is inversely proportional to its viscosity, hence gas injection for EOR is associated with high mobility ratios (low gas viscosities and high water/oil viscosities). This causes gases to effectively flow into zones with higher permeabilities and destabilize the displacement front by viscous fingering and gravitational segregation. The recovery of any reservoir fluid, E_{Ri}, can be calculated as the product of macroscopic displacement efficiency, E_{Vi}, and microscopic displacement efficiency, E_{Di}, from a displacement process [67]:

$$E_{Ri} = E_{Vi} \cdot E_{Di} \quad (4)$$

The interplay between capillary, viscous and gravitational forces affects the displacement efficiency. Ratio of viscous to capillary forces during a displacement process can be correlated to the residual oil saturation and is often described by the capillary number, N_C. N_C is a dimensionless semi-empirical parameter and can be expressed as [67]:

$$N_C = \frac{F_v}{F_c} = \frac{u\mu}{\sigma_{ij}} \tag{5}$$

where F_v is the viscous forces, F_c is the capillary forces and σ_{ij} is the IFT between injected fluid, i, and displaced fluid, j. The capillary number during a foam flooding process can be defined as [68]:

$$N_C = \frac{kk_{rf}\Delta P}{\sigma_{ow}L} \tag{6}$$

where k_{rf} is the foam relative permeability and L is the length of the porous media.

Capillary numbers from Equations 5 and 6 correlate to residual oil saturations in capillary desaturation curve plots [69, 70]. In general, higher capillary numbers reduce residual oil which in turn enhances oil recovery [67, 68, 71].

Surfactants and nanoparticles decrease the energy requirement to form foams, which can be conceptualized through [72]:

$$dE = \sigma_{wg}dA \tag{7}$$

where dE is the energy required to increase the surface area by dA. Hence, a large reduction in σ_{wg} reduces the overall energy requirement for foam generation. Once, adsorbed to an interface, the energy, E, required to desorb a spherical particle is given by [59]:

$$E = \pi R^2 \sigma_{ij}(1 \pm cos\theta)^2 \tag{8}$$

where R is the particle radius and θ is the contact angle. The sign in front of $cos\theta$ is negative when the particles are removed into the aqueous phase, otherwise it is positive.

1.5 Field Pilot Project

The field pilot project was initiated in January of 2015 with the primary objective of advancing CO_2-foam mobility control technology for EOR and CO_2 storage at the Norwegian continental shelf. The interdisciplinary effort is led by UiB and includes five other universities in the US and Europe (Stanford University, Rice University, the University of Texas at Austin, TU Delft and the University of Stavanger) and five energy companies (Shell, Total, Equinor, Tabula Rosa Energy and StableRock Energy), all contributing with expertise in different areas. The primary focus of the Reservoir Physics Group (UiB) has been to estimate foam efficiency (CO_2 storage potential, EOR effect, CO_2 mobility reduction) and deriving input to the numerical simulator for up-scaling.

Two field pilot sites with different reservoir material were selected as candidates, both located in West Texas, US. These choices were favorable from an economical and operational point of view, since they are onshore fields with a pre-existing CO_2 infrastructure and have a short inter-well distance. This reduces operational costs and time from foam injection to production response. The project development in East Seminole (ES, carbonate reservoir, Figure 3) has advanced faster than the one in Fort Stockton (sandstone reservoir) and is expected to start foam injection in early 2019. All of the numerical modelling efforts and most of the field specific laboratory investigations are performed on ES core material, with ES reservoir fluids and at ES reservoir conditions (Papers 2 and 3). A more detailed description of the ES field pilot project (reservoir geology, history, injection strategies, modeling and surface facilities) can be found elsewhere [73, 74].

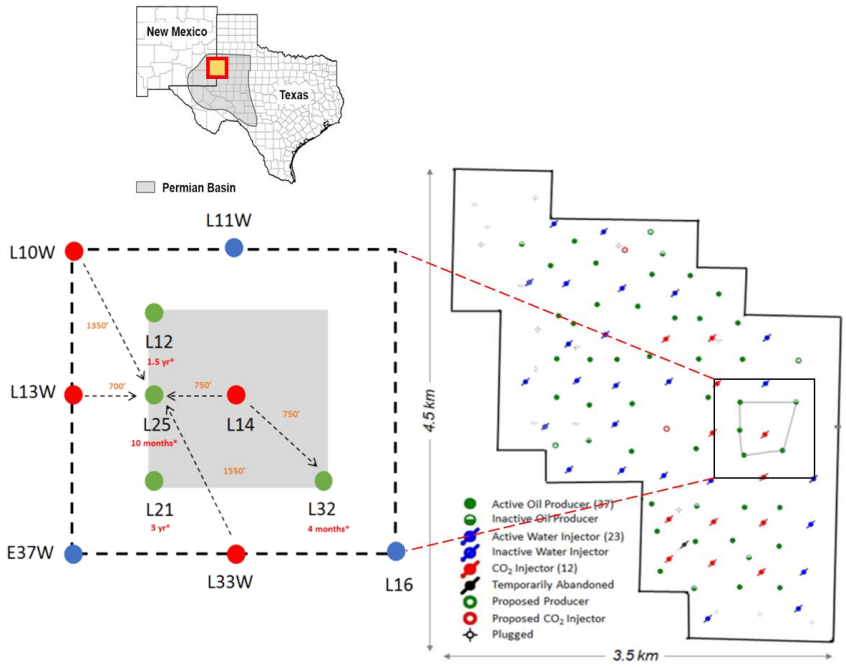

Figure 3: Map of the inverted 5-spot well pattern (gray shaded area) of the East Seminole carbonate field, located in the Permian Basin, West Texas. The well-pattern consists of one injector (L14, red dot) and four producers (L12, L25, L21 and L32, green dots).

1.6 Bottom-up Multi-Scale Approach

The scientific approach used to evaluate nanoparticle- and surfactant-stabilized CO_2-foam performance includes a multi-scale laboratory component and a field-scale numerical simulation component. Data collected during field-scale implementation of the laboratory tested foam system will form an optimal process for knowledge-building and enhance understanding related to the up-scaling approach. Emphasis is put on increasing the statistical significance of laboratory data by performing repeated experiments at equal conditions, thereby improving accuracy of reported results. Ultimately, this reduces decisional risks and improves the predictions from foam model simulations. In general, the approach attempts to establish casual links between input parameters and measured responses by: i) varying one parameter at a time; and ii) introducing one new variable at a time. The latter increases the overall complexity of the systems in a controlled manner. The process is illustrated in Figure 4.

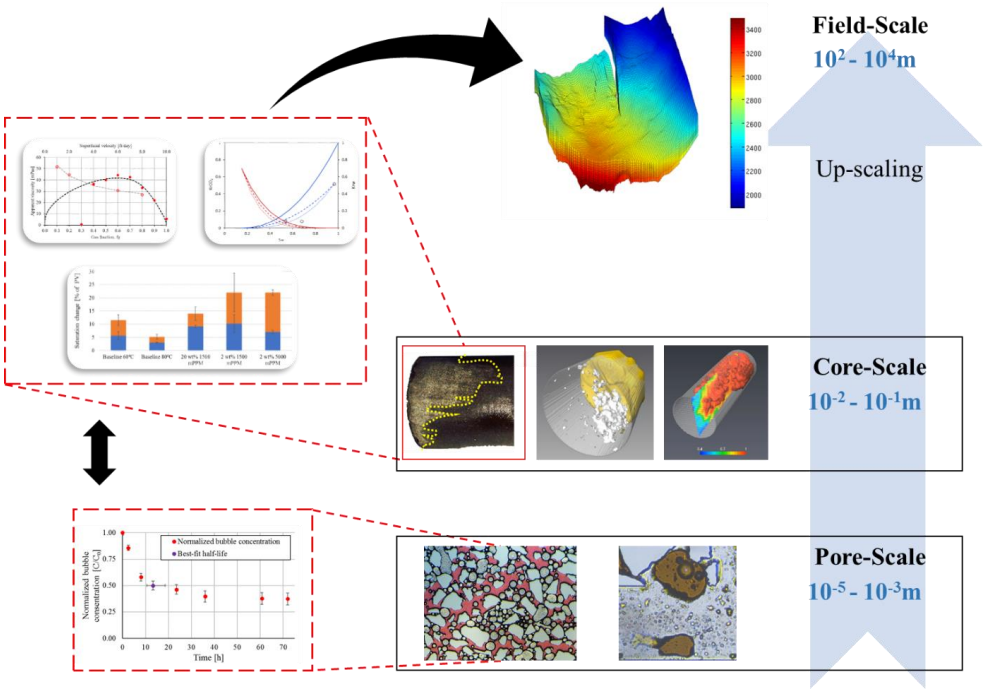

Figure 4: Illustration of the multi-scale approach implemented to describe CO_2-foam behavior in porous media and determine CO_2-foam performance. The integrated approach includes an up-scaling of complexity from pore-scale (micromodels) injections of foam without oil, to core-scale evaluation on reservoir material with oil. Numerical up-scaling is performed based on laboratory determined parameters for field implementation of the foam system.

1.6.1 Pore-Scale

By performing the investigations at the smallest scale relevant for the application of CO_2-foams (pore-scale), 2D silicon wafer micromodels enable direct visual observations of fluid flow, phase distributions and foam texture. Facilitating a controlled environment based on thin sections of realistic reservoir material, the micromodels include some of the complexity of reservoir porous media (aspect ratio, pore size distribution), while eliminating others (clay content, minerals and wettability alteration). The micromodels furthermore show high resistance to adverse effects from high-pressure co-injections of CO_2 and water (e.g. carbonate core plugs dissolve in the acidic environment). From a methodological point of view, the latter property is advantageous when evaluating different foam systems, as the porous media is invariable for all sets of experiments. This dissertation implements pore-scale observations mainly for qualitative foam evaluation (increased lamella generation from

adding foaming agents, foam transport and foam texture), but a procedure for evaluating static foam strength was developed and implemented.

1.6.2 Core-Scale

Implementing similar injection methods as described for pore-scale, injection in reservoir core plugs enables insight into the causal relationship between foam system parameters and data collection for input to simulation models. Quantitative evaluations of foam performance at this scale increase the overall understanding of foam floods and contribute to field pilot decision-making processes by determining injection strategy, surfactant concentration and slug sizes.

Foam scans

Foam scans (Papers 2, 3 and 4) are implemented to evaluate foam strength at different gas fractions (foam quality scans) and injection rates (foam rate scans) through apparent viscosity calculations (Equation 1). Saturation profiles during foam scans can be obtained based on average fluid saturations (Paper 4).

EOR floods

Co-injections of CO_2 and brine (with or without foaming agent) in tertiary EOR mode provide quantitative evaluation of foam performance based on incremental oil recovery, foam strength and CO_2 storage (Papers 2, 3, 5 and 6).

1.6.3 Field-Scale Modeling

Foam flow is modeled to determine the injection strategy for the field pilot and predict foam performance. There exists a wide variety of models that capture the mobility reduction effect of foams in porous media. These can be divided into population balance (PB) and local equilibrium (LE) models which differ in terms of their level of detail and complexity. PB models include the dynamics of foam flow on pore-scale (foam generation, destruction and trapping) to fully describe the governing dynamics of foam flooding [63, 75-77]. The advantages of PB models are that they yield a more comprehensive description of the foam dynamics. The high computational cost and laboratory challenges related to determine required input parameters, on the other hand, are considered drawbacks. LE models include foam effects through a gas mobility

reduction factor. Explicit analysis of foam dynamics are thus excluded. This indirect approach reduces the computational intensity, which is one of the main reasons why it was selected for the field up-scaling approach presented in this dissertation. Comparable results from foam modeling on both laboratory- and field-scale are reported in various studies [75, 78, 79]. All field simulations for this pilot project use a conventional reservoir simulator (ECLIPSE 300) with an embedded LE model [80]. The aggregate effect of foam is included by multiplying gas relative permeability, k_{rg}^{nf}, with a (modeling) mobility reduction factor (FM), obtaining gas relative permeability during foam flow, k_{rg}^{f} :

$$k_{rg}^{f} = k_{rg}^{nf} \cdot FM \tag{9}$$

FM incorporates the effects of water saturation, shear rate, surfactant concentration and oil saturation through different functions, F_i:

$$FM = \frac{1}{1 + fmmob \cdot \prod_{i=1}^{n} F_i} \tag{10}$$

where *fmmob* is a constant referred to as the *reference mobility-reduction factor* and is obtained from laboratory measurements (maximum apparent viscosity during foam quality scan, Paper 2). A more detailed description is given elsewhere [81, 82]. The laboratory determined results are included in the model by regression analysis obtained from minimizing the sum of the differences, $\psi(x)$, between experimental data points and the regression function [83]:

$$\psi(x) = \sum_{i=1}^{n} \left(\mu_{app,i}(x) - \mu_{app,i}^{exp.}\right)^2 \tag{11}$$

where x is the vector of foam model parameters, $\mu_{app,i}$ and $\mu_{app,i}^{exp.}$ are the apparent viscosities from the regression and laboratory experiments, respectively.

2. Results and Discussions

This section summarizes the pure CO_2 injections and field specific results for the East Seminole pilot (2.1) described in Papers 1, 2 and 3, the observations from nanoparticle-stabilized CO_2-foams (2.2) treated in Papers 4, 5 and 6 and CO_2 storage potential (2.3) discussed in Papers 2 and 6. A brief quantitative assessment of carbon negative oil production from CO_2-foams using nanoparticles and surfactants as foaming agents is included in Section 2.3. The bottom-up approach is implemented throughout this section. For direct pore-scale visualization, high-pressure silicon-wafer micromodels were implemented since they provide insight into foam texture, foam stability and fluid flow diversion. Foam generation and stability were evaluated with respect to foaming agents during dynamic and static conditions. The same CO_2-foam systems were tested in core plugs to evaluate foam behavior at different gas fractions (foam quality scans) and rates (foam rate scans) during co-injection. The final laboratory approach included foam injections in core plugs saturated with oil to quantify foam performance in terms of stability, EOR and CO_2 storage. Numerical simulations evaluated foam performance on field-scale based on laboratory derived input data.

2.1 CO_2-Foam from Lab-to-Field

Developing field specific CO_2-foam systems requires a comprehensive understanding and testing of multi-phase flow in porous media. Obtaining input for numerical modelling requires use of field fluids and material at field conditions, wherever possible.

2.1.1 CO_2 Injection for EOR and CO_2 Storage

Main results (Paper 1) include:

- CO_2 flows through tight shale oil core plugs without introducing fractures
- Unstable CO_2 fronts cause early breakthrough and low sweep

Continuous CO_2 injections for EOR in tight shale oil reservoir core plugs were investigated in Paper 1. Implementing water injection for EOR in unconventional tight reservoirs is less efficient compared to conventional reservoirs due to the ultra-low

permeability associated with matrix composed of micro- and nano-pores. The injections were performed without introducing fractures to the reservoir rock with inlet pressures of 22 MPa and temperatures of 60ºC. Results demonstrate the feasibility of utilizing CO_2 flooding as a recovery mechanism in shale oil formations and that CO_2 displaced oil during differential pressure driven EOR, at laboratory scale. Observations indicate unstable displacement front, low sweep and early CO_2 breakthrough indicative of gas channeling (Figure 5). This is likely related to the high mobility ratio between injected CO_2 and displaced crude oil.

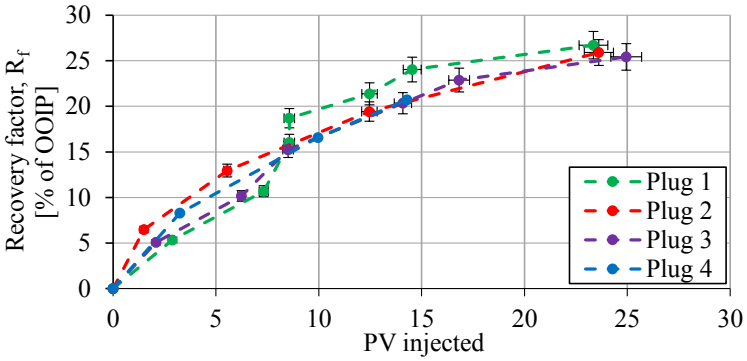

Figure 5: Oil recovery factor as a function of pore volume CO_2 injected during CO_2-EOR in four reservoir shale oil core plugs. Early CO_2 breakthrough was observed, indicative of gas channeling.

Recovery profiles (Figure 5) suggest low viscous displacement in the early stages of injection and an oil production dominated by diffusion. Diffusion dampens the adverse effects of viscous fingers and gas channeling, explaining the prolonged tail production. Visual observations of produced oil color from experiments with different injection time and system size (large system, longer injection time: three core plugs stacked in succession; small system, shorter injection time: single core plug) corroborated oil displacement from diffusion. Heavier components (darker oil) were produced from longer injection time (large system injection time: 117 hours) compared to lower injection time (single core: 6 hours) (inset, Figure 6) [84]. On a larger scale, diffusion is perceived to be slower than capillary and viscous driven displacement processes. It is, however, spontaneous, something which causes it to be continuous and ubiquitous [85].

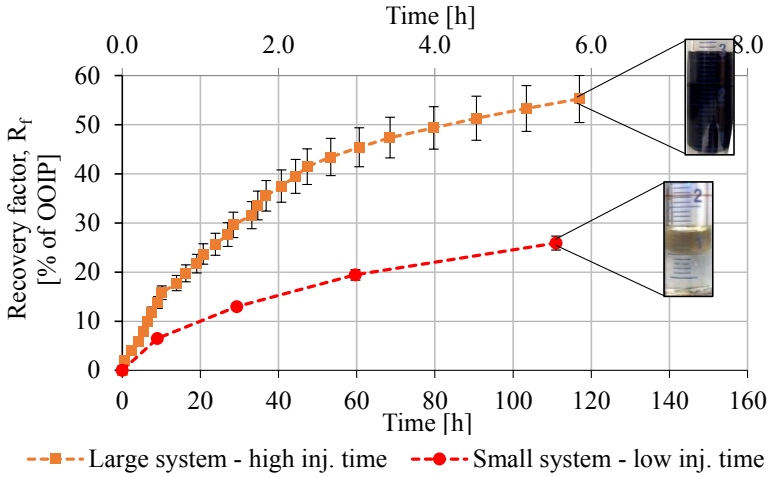

Figure 6: Oil recovery factor as a function of pore volume CO_2 injected for a large system (high injection time, primary horizontal axis) and a single core plug (low injection time, secondary horizontal axis). Differential pressure is constant over the systems, hence the pressure gradient for the single core plug was ~3 times higher than the large system. Earlier CO_2 breakthrough and a lighter oil composition were observed (inset), corroborating increased miscibility from diffusion as the main recovery mechanism on core-scale (increased CO_2 exposure time).

On average, single core injections yielded a final oil recovery $R_f = 31.9 \pm 6.1\%$ of OOIP after injecting 24.7 ± 4.3 PV CO_2 (average injection time of 22.0 ± 2.9 hours) for 12 injection tests, compared to $R_f = 55.3 \pm 8.7\%$ of OOIP after injecting 3.4 ± 0.2 PV CO_2 (injection time of 117 hours) for one injection test in a large system. Additional recovery is assumed to mainly occur from the developed multi-contact miscibility caused by molecular diffusion, shown to be an efficient CO_2-EOR mechanism at core-scale [86].

2.1.2 CO_2-Foam at Pore-Scale

Main results (Paper 2) include:

- Verification of foam generation, CO_2 mobility reduction and flow diversion from pre-selected surfactant
- Developing a method for determining *in-situ* performance of foaming agents

As part of the integrated approach to test and up-scale a foam system for field implementation, high-pressure silicon-wafer micromodels were used for pore-scale visualization. This provides direct insight into foam performance from foam texture,

foam stability and CO_2 mobility reduction during flow. It therefore verifies the ability of the foam system to generate and stabilize lamellae at elevated pore pressures with reservoir brines.

A baseline (co-injection of brine and CO_2 at $f_g = 0.70$) flow test was performed to evaluate phase distributions in a two-phase system without a foaming agent. Visual observations showed few CO_2 bubbles and a gas phase spanning several pores without being separated by lamellae (Figure 7). Most of the observed lamellae is caused by leave-behind from CO_2 displacing water (Section 1.4.2), a configuration characterized by low CO_2 mobility reduction [25, 38].

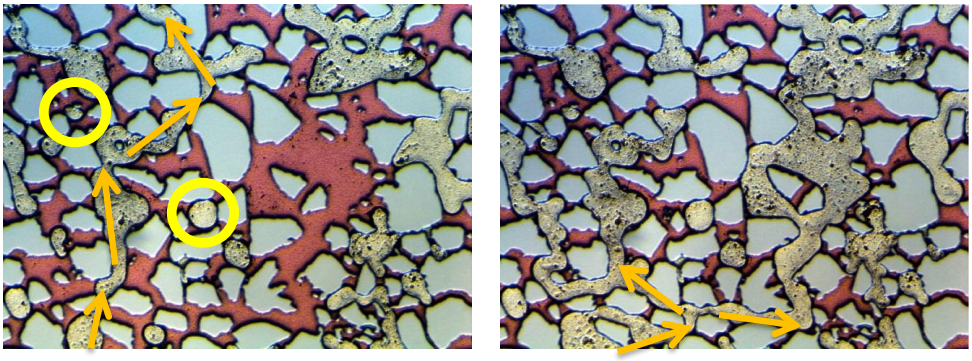

Figure 7: Baseline co-injection of brine and CO_2 at 9.0 MPa and 20ºC with a constant gas fraction of 0.70. The light blue regions are solid grains, water phase in red and CO_2 in gray. Continuous CO_2 phase spanning several pores suggested limited CO_2 mobility reduction and lamellae generation by leave-behind mechanism. The orange arrows indicate CO_2 flow zones within the field of view. Water primarily saturated smaller pores and was continuous throughout the pore space, whereas CO_2 flow occurred in the medium to large pores. Isolated CO_2 bubbles are indicated with yellow circles.

The effect of adding SurfA to the brine (C_{surf} = 1 wt%) was evaluated by performing co-injections at the same conditions as for the baseline. A strong CO_2-foam was generated with high bubble concentration indicative of high CO_2 mobility reduction (Figure 8) [37, 60, 61]. In contrast to baseline, several CO_2-in-water bubbles occupied each pore and the gas phase did not span across several pores.

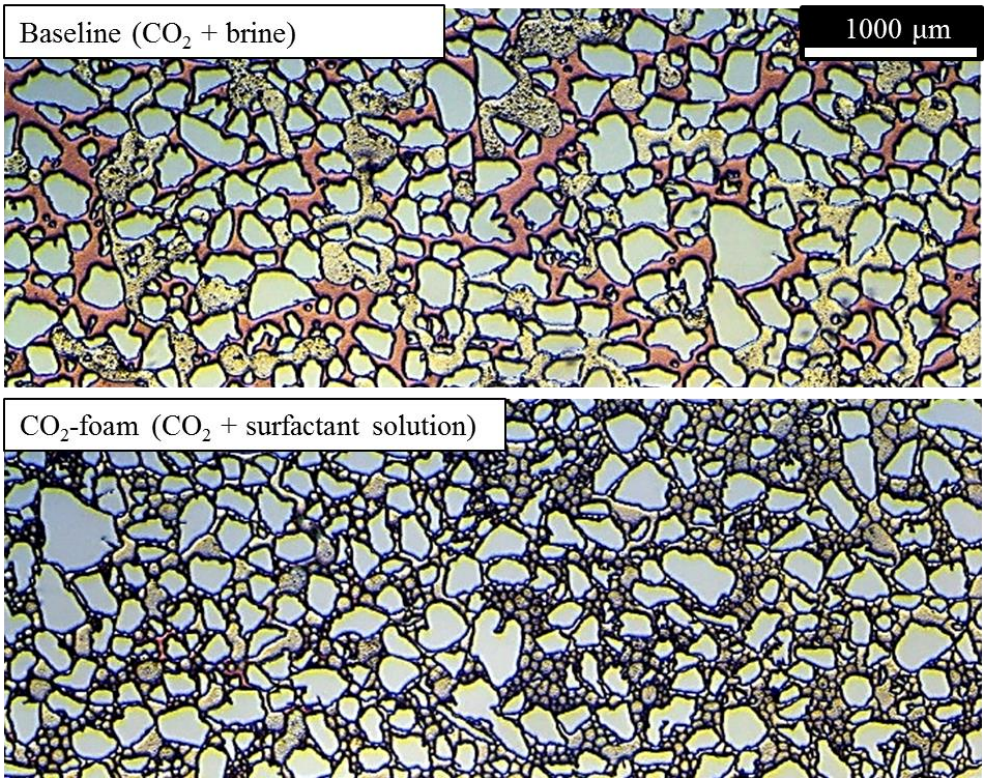

Figure 8: Comparison between co-injection without (top) and with (bottom) SurfA. The light blue regions are solid grains, water phase in red and CO_2 in gray. Co-injections performed at 9.0 MPa and 20°C with a constant gas fraction of 0.70. Compared to baseline, bubble concentration is 2-3 orders of magnitude higher for the surfactant-stabilized CO_2-foam, implying high gas mobility reduction.

Static stability

Increased stability from foaming agents can be quantified by half-life measurements [87, 88]. The method is often implemented on bulk foams situated in foam columns where half-life is defined as the time it takes for a static foam to reduce its height by 50%. Effect of foaming agent concentration and oil composition can be evaluated based on differences in half-life times [89]. To determine the static foam strength at elevated pressures, rate of foam coalescence was measured during static conditions in micromodels, for 72 hours. Normalized bubble concentration (ratio of bubble concentration to initial bubble concentration) in the field of view was used to quantify foam stability through half-life calculations (Figure 9). This approach enables direct quantitative comparisons between foaming agents in a porous media at elevated

pressures. It furthermore allows the effects of foaming agent concentration, brine composition and oil saturation to be investigated with respect to foam stability (this, however, is not included in this dissertation). Observations showed a decreasing rate of coalescence over the first 35-40 hours before asymptotically approaching a constant normalized bubble concentration of 0.37 ± 0.06, with a half-life of 13.6 ± 4.0 h.

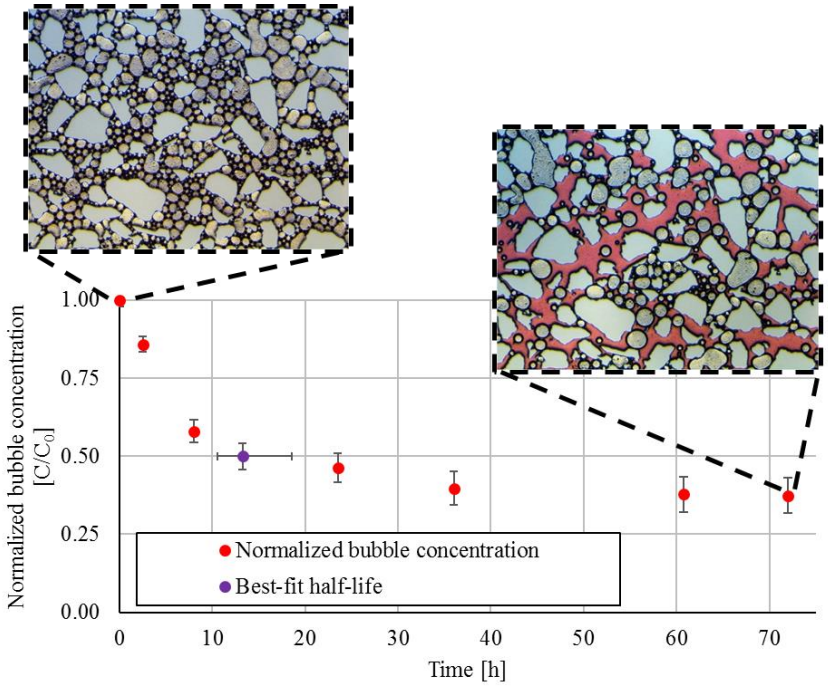

Figure 9: Normalized bubble concentration (red dots) in field of view as a function of time, at static (no-flow) conditions. Purple dot represents the foam half-life, calculated from a best-fit regression analysis. Inset pictures show foam texture at beginning (0h) and end (72h) of the static test. The light blue regions are solid grains, water phase in red and CO_2 in gray.

Flow diversion from CO_2-foam

During co-injections with surfactant, CO_2-foam generation was shown to block-off an existing flow zone and divert fluid flow elsewhere (Figure 10). Several cycles of brine and CO_2 propagated in an alternating sequence through the "high flow zone" (yellow rectangle, Figure 10). Picture D captures high CO_2 and brine flow, within the same zone, resulting in a high foam generation (picture E). Local static conditions were established for ~7 minutes, during which a total of ~12 PV were injected. This suggest CO_2-foam block-off with resulting fluid flow diversion at pore-scale.

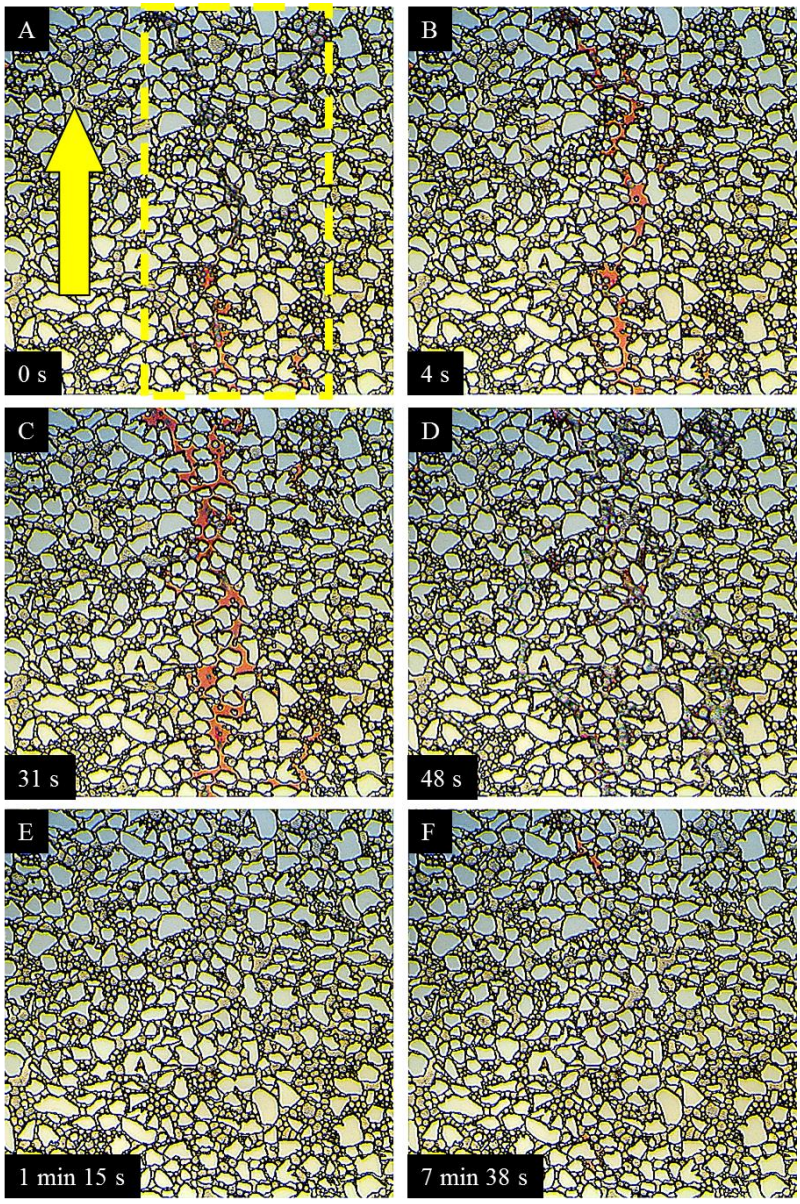

Figure 10: Block-off and flow diversion as a result of CO_2-foam generation at pore-scale. The light blue regions are solid grains, water phase in red and CO_2 in gray. A-C show a flow zone (yellow dotted rectangle) gradually filling with water. Yellow arrow indicates direction of flow. CO_2 and water flowed simultaneously (D) before a high bubble concentration foam was generated (E). No flow was observed for ~7 min, implying that injected fluids were diverted away from field of view, due to foam. A total of 12 PV were injected between E and F.

2.1.3 CO_2-Foam at Core-Scale

Main results (Papers 2 and 3) include:

- Surfactant concentration (C_{surf} = 0.5 wt%), injection strategy (rapid SAG) and slug sizes (average gas fraction set to 0.70) were determined for the field pilot
- Foam system shows high gas mobility reduction and shear-thinning behavior
- Simulations indicate favorable foam responses in field

The foam system were tested in core plugs to evaluate foam strength at different gas fractions and injection rates, before being implemented on core plugs saturated with oil to evaluate foam performance with regards to EOR efficiency and CO_2 storage. All injections were performed at reservoir temperature and pressure (~17.5 MPa and 40ºC) with reservoir fluids.

Foam scans

Foam scans were performed to evaluate foam strength and flow behavior at different gas fractions (*foam quality scan*) and injection rates (*foam rate scan*). The former scan gives information about the foam strength at different steady-state gas fractions (constant injection rate), whereas the latter scan relates to the rheological properties of the foam in porous media (constant gas fraction). Results from both sets of experiments are directly implemented in the simulation model. Foam scans used a drainage-like injection sequence: co-injection of CO_2 and brine with a monotonic increasing gas fraction or injection rate. The foam rate scan shows that the foam was shear-thinning (non-Newtonian) where apparent foam viscosity decreased with increasing injection rate (Figure 11) [65]. This is favorable during field injection because it reduces the risk of injectivity problems related to pressure build-up in the near-well region and promotes in-depth mobility control. The injection rate for foam quality scans was selected based on the highest apparent viscosity during the foam rate scan, *i.e.* a superficial velocity of 1.0 ft/day (Figure 11).

To evaluate mobility reduction from foam injection a baseline co-injection was performed at the same conditions, without SurfA. The highest apparent viscosities, i.e. strongest foam [90, 91], were obtained with an apparent viscosity of 44.3 mPas and 1.8 mPas at f_g = 0.60 and f_g = 0.50 for surfactant and baseline co-injections, respectively.

The mobility reduction factor (MRF) during foam injections were 25.5 ($f_g = 0.60$) and 25.4 ($f_g = 0.70$).

Laboratory injections are performed as co-injections to promote steady-state flow conditions, whereas a surfactant alternating gas (SAG) injection sequence will be implemented in the field. Gas fractions measured on core-scale are analogue to the average gas fraction (in each slug-sequence) at field-scale. The insignificant reduction in MRF from increasing gas fraction ($f_g = 0.60$ to $f_g = 0.70$) reduces surfactant usage (and cost) at field-scale (25% reduction). A macroscopic average gas fraction of 0.70 was therefore selected for the field pilot slug sizes.

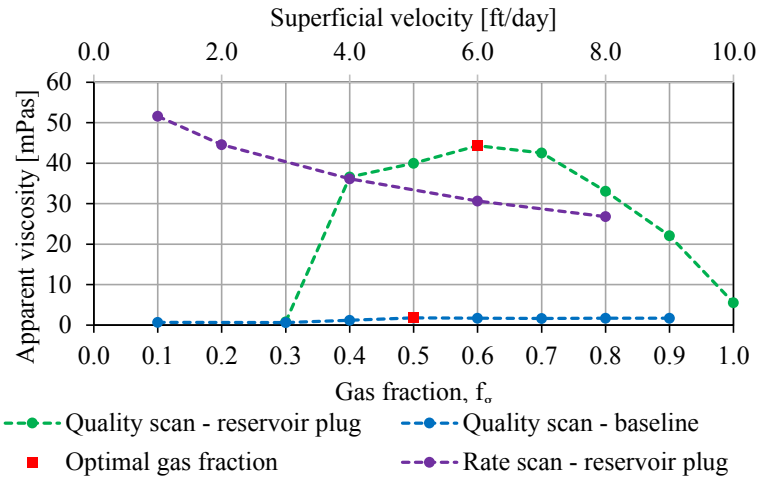

Figure 11: Apparent viscosity (primary vertical axis) as a function of superficial velocity (purple: secondary horizontal axis) and gas fraction (green and blue: primary horizontal axis) during drainage-like co-injection of CO_2 and brine. Blue: baseline quality scan, co-injection of brine and CO_2 at fixed injection rate (1 ft/day). Green: surfactant-stabilized foam quality scan, co-injection of surfactant solution and CO_2 at fixed injection rate (1 ft/day). Optimal gas fraction is defined as the maximum apparent viscosity and is represented with a red square, indicating $f_g = 0.60$ as the optimal gas fraction for foam injection in reservoir rock. CO_2-foam shows shear-thinning behavior (purple: secondary horizontal axis) during co-injections with constant gas fraction ($f_g = 0.70$).

Surfactant concentration

Surfactant usage has a major impact on the financial evaluation of foam injections on field-scale. Two sets of experiments (with surfactant concentrations of 0.5 and 1.0 wt%) were performed in reservoir core plugs to determine the surfactant concentration for field injections: i) foam quality scans with oil (oil saturation at approximately S_{or});

and ii) tertiary CO_2-foam injections for EOR. Foam quality scans enable direct comparison between foam strength and surfactant concentrations, while EOR injections evaluate foam performance with respect to foam strength and incremental oil production.

The foam quality scans were performed on aged reservoir core plugs after tertiary CO_2-foam injection for EOR to replicate field conditions. The results (Figure 12) display reduced foam strength with lower surfactant concentration (apparent viscosity is reduced by ~35%). With a monotonically decreasing foam strength as a function of gas fraction, the foam behavior differs significantly from foam scans in the water-wet reservoir core plug (Figure 11). This discrepancy is related to the change in initial conditions (wettability and fluid saturations), where foam strength is known to be adversely affected by oil [64] and reduced water wetness [35]. Due to the injection sequence (foam scans initiated after tertiary CO_2-foam injection), hysteresis effects related to gas saturation are likely present and have demonstrated an ability to alter foam behavior (see discussion on hysteresis effects in Paper 4 and Section 2.2.2).

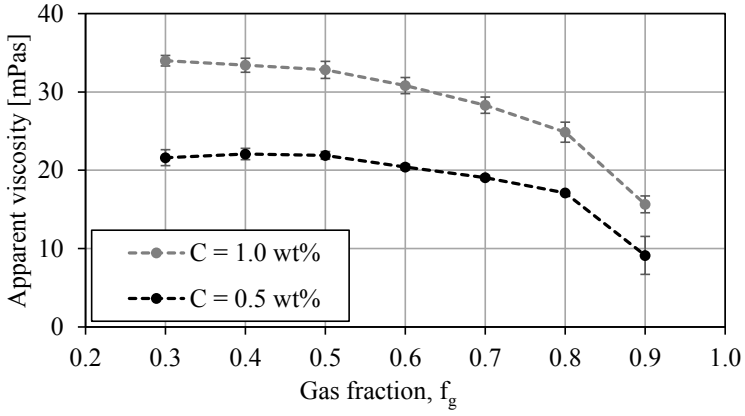

Figure 12: Average apparent viscosity as a function of gas fraction during drainage-like co-injection of CO_2 and surfactant solution with concentrations of C_{surf} = 1.0 wt% (gray, two injection tests) and C_{surf} = 0.5 wt% (black, three injection tests). Error bars: uncertainties as standard error from the mean.

CO_2-foam injections in reservoir core plugs were performed with the same surfactant concentrations (C_{surf} = 0.5 wt% and 1.0 wt%) and evaluated with respect to: i)

incremental oil recovery during tertiary EOR; and ii) pressure gradient increase (ratio of pressure gradient at the end of foam injection to pressure gradient at the end of water injection). A pure CO_2 injection was performed as a baseline for comparison, and gas fraction was held constant at $f_g = 0.70$ during co-injections. No adverse effects on incremental oil recovery ($\Delta R_f = 29.2 \pm 1.6\%$ of OOIP with $C_{surf} = 1.0$ wt% and $\Delta R_f = 28.5 \pm 2.8\%$ of OOIP with $C_{surf} = 0.5$ wt%) or foam strength ($\Delta P/m$ increase = 264 ± 48% with $C_{surf} = 1.0$ wt% and $\Delta P/m$ increase = 301 ± 94% with $C_{surf} = 0.5$ wt%) were observed from a reduction in surfactant concentration (Figure 13).

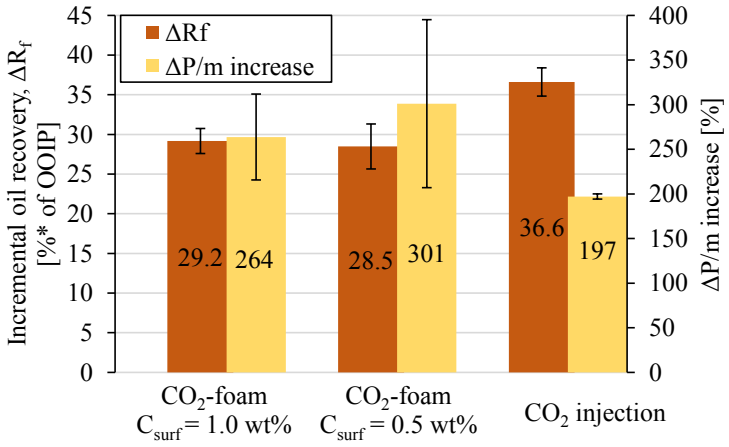

Figure 13: Incremental oil recovery and corresponding increase in pressure gradient during foam injection with C_{surf} = 1.0 wt% (two injections tests) and C_{surf} = 0.5 wt% (three injection tests). Pure CO_2 injection (one injection test) is included as baseline for comparison. Uncertainties are given as standard error from the mean value when the number of injection tests, N, is larger than 1, and as measurement uncertainty when N=1.

A higher incremental oil recovery with a lower corresponding pressure gradient increase was observed from the pure CO_2 flood (Figure 13). The effect of CO_2 diffusion is larger at core-scale compared to what is expected at field-scale, mainly due to there being a high surface area to bulk volume and smaller system size (Paper 1, Section 2.1.1). In addition, co-injections are expected to increase water shielding (water-films between CO_2 and oil [92, 93]) which reduces CO_2-oil contact area and adversely affects the rate of miscibility development.

Reducing the surfactant concentration from C_{surf} = 1.0 wt% to C_{surf} = 0.5 wt% decreased foam strength during foam quality scans at low oil saturation (Figure 12). This reduction is not observed to transfer to or reduce efficiency of tertiary CO_2-foam injections for EOR in reservoir core plugs. Based on the obtained experimental data (and financial considerations), the field pilot surfactant concentration was determined to be 0.5 wt% SurfA in brine. CO_2 to brine slug size ratio (during SAG injections in the field) was set to 70% based on foam quality scans.

2.1.4 CO_2-Foam at Field-Scale

To establish a field-scale injection strategy, parameters from laboratory experiments (rate scan, quality scan and end-point relative permeability measurements) must be integrated with the history matched dynamic reservoir model (Paper 3). Four simulation cases were carried out to determined slug sizes (Figure 14). The foam performance was evaluated with respect to gas-oil ratio (GOR), CO_2 utilization factor (UF_{CO2}), CO_2 mobility reduction and incremental oil recovery. The simulations included a (baseline) water alternating gas (WAG) and three SAG injections with different slug sizes; single cycle (big), rapid cycle (small) and multi-cycle (medium) (Paper 3). Simulations indicated favorable effects from foam (Figure 14). Oil recovery estimates are highly sensitive to CO_2 volumes injected, which is adversely affected by increased injectivity during SAG. More accurate predictions of injectivity reduction can be obtained when actual field data (from the first SAG cycle) are available.

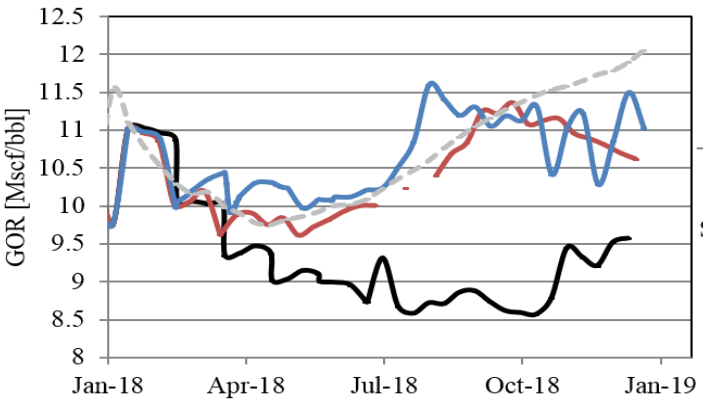

Case	UF_{CO2}
WAG	30
SAG	19
Single Cycle SAG	20
Rapid SAG	21

Figure 14: Left: one year field GOR for WAG (gray), multi-cycle SAG (black), rapid SAG (blue) and single cycle SAG (red). Right: CO_2 utilization factor (Mscf/bbl) for the different injection strategies.

2.2 Nanoparticles for CO_2-Foam

This section summarizes the work to evaluate nanoparticles as possible foaming agents in sandstones, where the dissertation focuses on two aspects of the used nanoparticles. Firstly, the physiochemical properties of the nanoparticles are characterized in aqueous suspensions (nanofluids). This includes measuring nanoparticle size distributions, nanofluid stability and nanoparticle effects on IFT. Secondly, the nanoparticles are evaluated in terms of their behavior in porous media. This includes retention analysis and quantifying their performance as foaming agents in CO_2-foam floods. A similar bottom-up approach as presented in Section 2.1 is implemented, *i.e.* the total system complexity is developed by a gradual introduction of new parameters or increasing system size (from pore-scale to core-scale). Foam performance was evaluated with respect to incremental oil recovery, foam strength and CO_2 storage, where nanoparticle-stabilized foams were compared to surfactant-stabilized foams (using AOS surfactant (Paper 4) and SurfA, Section 1.4.1).

Two nanoparticles (NPA: hydrophilic and NPB: less hydrophilic) were used in this dissertation. NPA is a commercially available silane modified colloidal silica, Levasil CC301 (illustrated in Figure 15). The modification produces a hydrophilic surface and a steric stabilization, resulting in an increased salt stability compared with unmodified silica particles. NPB is also silane modified, but less hydrophilic compared to NPA, and only used during tertiary EOR injections due to poor performance (Paper 5).

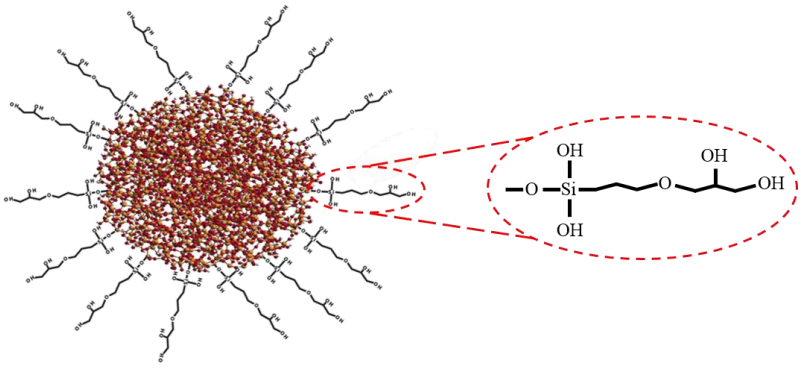

Figure 15: Illustration of the silane modified nanoparticle A. Published with permission from Nouryon.

2.2.1 Nanoparticle and Nanofluid Characterization

Main results include:

- Asymmetric nanoparticle size distributions with mean diameter ~20 nm
- SurfA reduces IFT (oil/water) more than nanoparticles

Foam stability is dependent on nanoparticle size, where smaller nanoparticles have a higher propensity to stabilize lamellae [94, 95]. The effect of nanoparticle size on foam strength can be understood through Equation 8, where the energy required to desorb a particle from an interface is proportional to the square of the particle radius. A larger radius increases the energy required to remove the nanoparticle from an interface. This implies that the energy required for nanoparticles to migrate to the interface is inversely proportional to their size [96-98]. In addition, the nanoparticle size and their size distribution give information about the likelihood of mechanical trapping in pore throats during flow in porous media. From dynamic light scattering, size distributions show a mean nanoparticle diameter of 23.3 nm (standard deviation, SD = 7.9 nm) and 20.3 nm (SD = 6.8 nm) for NPA and NPB, respectively. The size distributions are slightly asymmetrical, indicated by the right-skew in Figure 16.

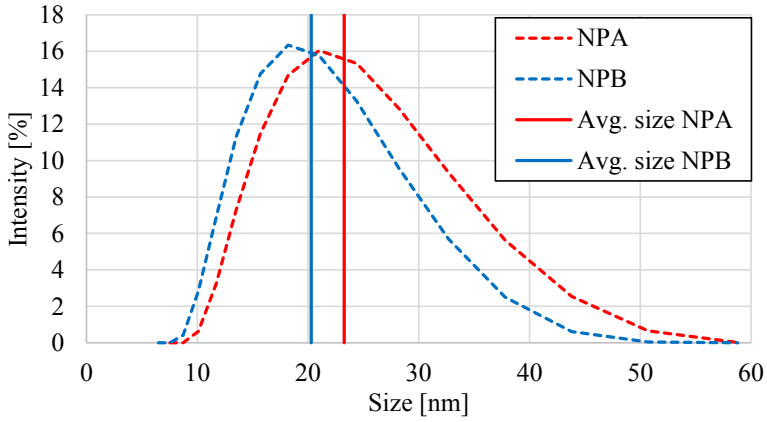

Figure 16: Size distribution of 0.5 wt% NPA and NPB dispersed in brine with 2 wt% NaCl. Measurement from dynamic light scattering at room temperature based on intensity (%).

EOR performance from nanofluids is related to the IFT between the fluids (Equations 5 - 8). IFT was measured in water/oil- and water/air-systems at ambient conditions using dispersions of NPA, NPB and SurfA in brine. Water/air measurements were

performed with the du Nouy ring method (KSC Sigma 700 force tensiometer) and water/oil measurements with the pendant drop method (OCA 20 measuring device). Results showed that the IFT reduction was highest for the surfactant (85 ± 21%), followed by NPB (54 ± 3%) and NPA (5 ± 1%) for concentrations ranging from 0 to 1 wt% (Figure 17). An IFT reduction of ~20% was observed in water/air-systems with nanoparticle concentrations ranging from 0 to 1 wt%.

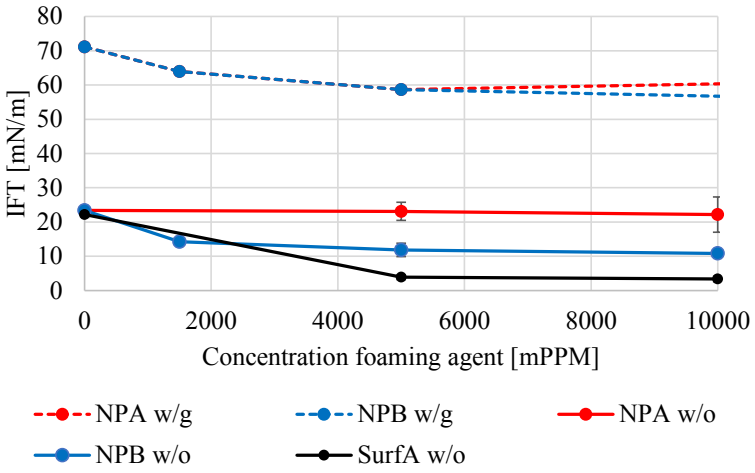

Figure 17: IFT in water/oil- and water/gas-systems for aqueous dispersions of brine and foaming agents at different concentrations (1 wt% = 10 000 mPPM). Error bars: uncertainties as standard error from the mean.

Nanofluid stability

Temperature, salinity, and pH have a direct effect on the interaction between nanoparticles and can result in aggregation and nanofluid instability [99]. Instability can lead to injectivity reduction (formation of highly viscous nanofluid or nanoparticle trapping in the near-well area) and reduced ability to stabilize foam lamellae. In general, nanoparticle aggregation depends on: i) salt concentration (aggregation occurs above a critical salt concentration); ii) temperature (critical salt concentration decreases with increasing temperature); iii) pH of the solution (aggregation is reduced with pH reduction); and iv) nanoparticle concentration (aggregation increases with increased nanoparticle concentration). To evaluate the stability of NPA, static and dynamic stability tests were performed at different conditions (Paper 6). The results indicate

(Table 1) high stability of NPA at concentrations from 0.15 - 0.50 wt%, in brines with NaCl concentrations up to 20 wt% and $CaCl_2$ concentrations up to 5.0 wt% at different temperatures (20ºC - 120ºC).

Table 1: Stability of NPA in brines at static and dynamic conditions.

Condition	NPA concentration [mPPM]	Salt composition	Salt conc. [wt%]	Temp [ºC]	Duration [days]
Static	1500, 3000, 5000	NaCl	2, 5, 10, 15, 20	40	75
		NaCl	2, 5, 10, 15, 20	20	90
		$CaCl_2$	1.5		
Dynamic	3000	NaCl	15.0	20	15.7
		NaCl	15.0	20	3.9
		$CaCl_2$	1.5	20	
		NaCl	15.0	20	2.7
		$CaCl_2$	5.0	20	
		NaCl	20.0	20	3.9
		$CaCl_2$	5.0	20	
		NaCl	2.0	120	0.8
		NaCl	2.0	60	0.8

2.2.2 CO_2-Foam at Pore-Scale by Nanoparticles

To determine foam response (generation and stability) of adding NPA to brine, direct pore-scale evaluation of foam texture and generation was implemented during co-injection without oil (as described in Sections 1.6.1, 2.1.2 and Paper 2). Fluids were injected with a constant gas fraction of 0.70, at 90 bar, temperatures of 20ºC and a NPA concentration of 0.15 wt%. The observations were compared to baseline co-injections (without a foaming agent) and co-injections with surfactant solution (1 wt% SurfA). Visual comparisons between baseline and NanofluidA injections showed no significant effect in terms of foam generation when adding NPA to the brine (Figure 18). Occasional appearances of small CO_2-in-water bubbles, however, (very low bubble concentration per unit area compared to surfactant-stabilized bubble concentrations) were observed (yellow arrow, Figure 18). The bubbles were smaller than bubbles occurring during baseline injections (Figure 7), suggesting that they might be caused by the nanoparticles. Low bubble concentration for multiple injection tests, indicates no ability to reduce CO_2 mobility in these experiments.

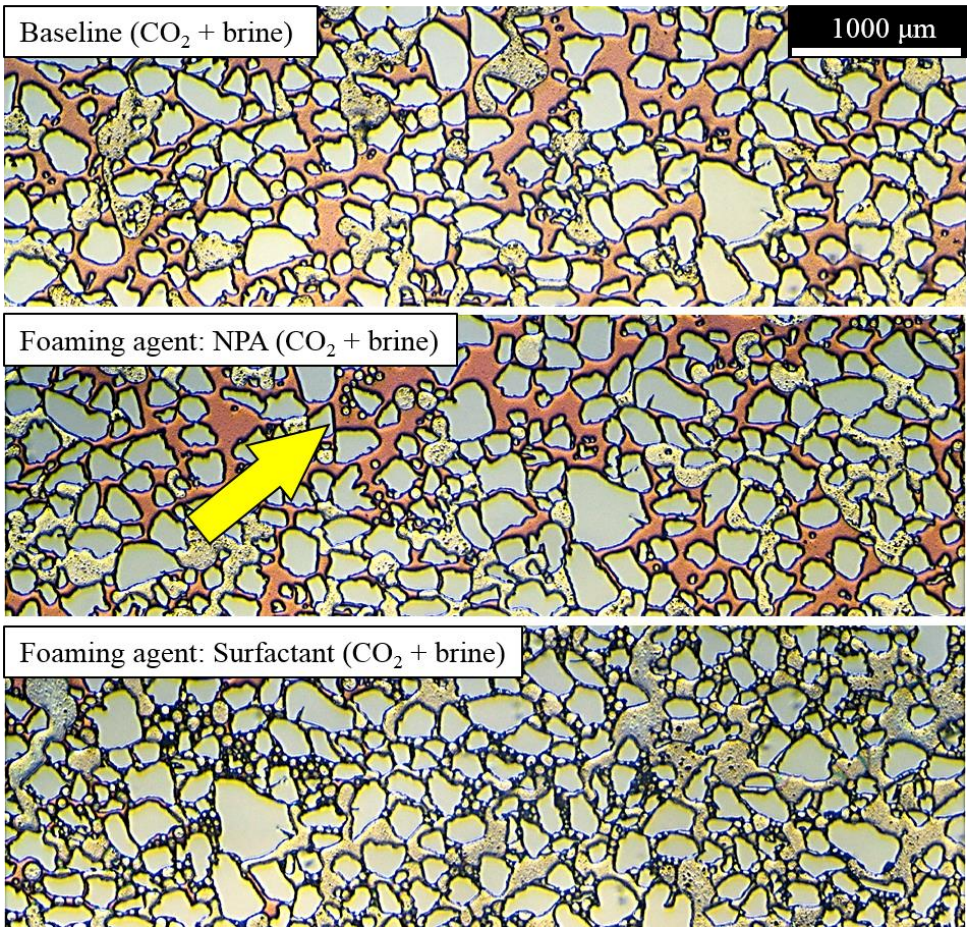

Figure 18: Direct evaluation of foam texture and generation during co-injection of CO_2 and brine (with or without foaming agent) at fixed gas fraction (f_g = 0.70), pore pressures of 90 bar at 20ºC. The light blue regions are solid grains, water phase in red and CO_2 in gray. NPA (0.15 wt%) showed no foam generation compared to baseline, whereas SurfA (1 wt%) generated strong foams with high bubble concentration. Yellow arrow points to an occasional occurrence of CO_2-in-water bubbles, significantly smaller than the observed bubbles during baseline injections.

2.2.3 CO_2-Foam at Core-Scale by Nanoparticles

Main results (Papers 4 and 5) include:

- Nanofluids flow unrestricted through sandstones with low retention
- The nanoparticles generate CO_2-foam during foam scans without oil
- Surfactant-stabilized foams are several times stronger than nanoparticle-stabilized foams during foam scans without oil

- In presence of crude oil, surfactant-stabilized foams collapse
- Nanoparticles display stabilizing effects in presence of crude oil

Retention

Using nanoparticles for CO_2-foam applications in porous media depends on their ability flow relatively unhindered through the reservoir. Retention is a measure of total particle loss to the formation and was evaluated from effluent production analyses during single-phase nanofluid injections (Papers 4 and 6). Retention incorporates the effects from: i) adsorption: particles adhering to the pore walls; ii) mechanical trapping: particle flow is blocked due to narrow pore throats; iii) gravitational settling: low flow rate relative to density differences between particles and aqueous phase results in a downward particle migration; iv) log-jamming: pore blocking by two or more particles with an individual size smaller than pore throat; and v) gelification: particles being trapped due to formation of highly viscous, no-flow, gels [100-102]. The total retention was calculated as the ratio of retained particles (mg) to the mass of the core plug (g) and measured at 20ºC and 120ºC, to evaluate the effect of temperature (Figure 19).

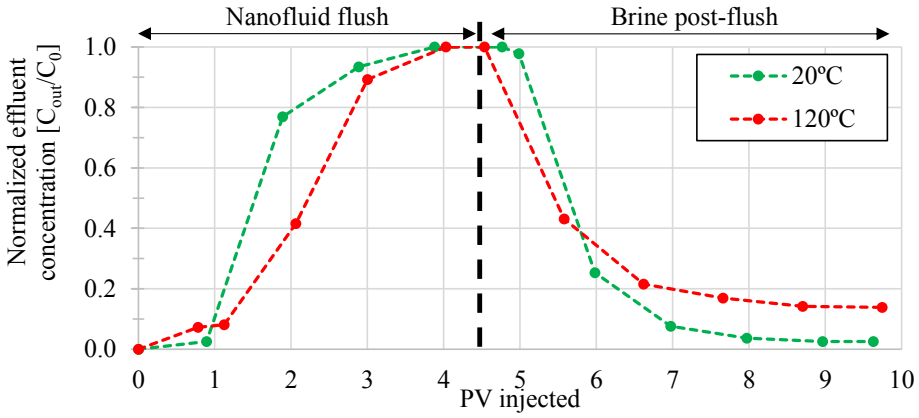

Figure 19: Normalized nanoparticle concentration at the effluent as a function of PV injected in sandstone core plugs. Pore pressure of 1 bar and temperatures set to 20ºC and 120ºC. To the left of the vertical dashed black line: nanofluid with a nanoparticle concentration of 1500mPPM is injected at a constant volumetric rate of 50 mL/h (superficial velocity of ~ 2 ft/day). At ~ 4.5 - 4.7 PV injected, fluid is changed to brine (0 mPPM nanoparticles) and a post-flush is commenced at the same injection rate for an additional ~ 4.7 – 5.2PV (to the right of vertical dashed black line).

Total retention was 0.40 mg/g at 20ºC (Paper 4) and 0.53 mg/g at 120ºC (Paper 6), showing a higher degree of particles retained (32%) with a six-fold increase in

temperature. Measured retention is similar to prior reported research in sandstones [103, 104], where the conversion factor from mg/g to mg/m^2 was selected as the specific surface area, 0.347 m^2/g, reported elsewhere [105]. Elution (ratio of particles re-mobilized during post-flush to mass of retained particles) was measured to 0.17 and 0.19 at 20ºC and 120ºC, respectively. This means that close to 20% of the retained particles are re-mobilized during the post-flush. Adsorption of SurfA on carbonate minerals is 0.9 mg/m^2 (~0.77 mg/g) at 80ºC, reported elsewhere [48].

Foam scans

Foam scans were performed with a nanofluid concentration of NPA of 1500 mPPM at temperatures of 20ºC and 90 bar pore pressures to evaluate nanoparticle-stabilized CO_2-foam strength and flow behavior at different gas fractions and injection rates. Foam was generated *in-situ*, and the effect of hysteresis was evaluated by implementing two different injection strategies: i) drainage-like flow sequence (co-injections with a monotonic increasing gas fraction from 0.1 to 1.0); ii) imbibition-like flow sequence (co-injections with a monotonic decreasing gas fraction from 1.0 to 0.1). From foam quality scans the main results showed that (Figure 20): i) NanofluidA generated and stabilized CO_2-foam; ii) near-Newtonian foam behavior; and iii) optimal gas fraction at f_g = 0.70, with a MRF of 2.8 (120 mL/h: 8.5 ft/day), 3.8 (180 mL/h: 12.7 ft/day) and 3.7 (240 mL/h: 16.9 ft/day).

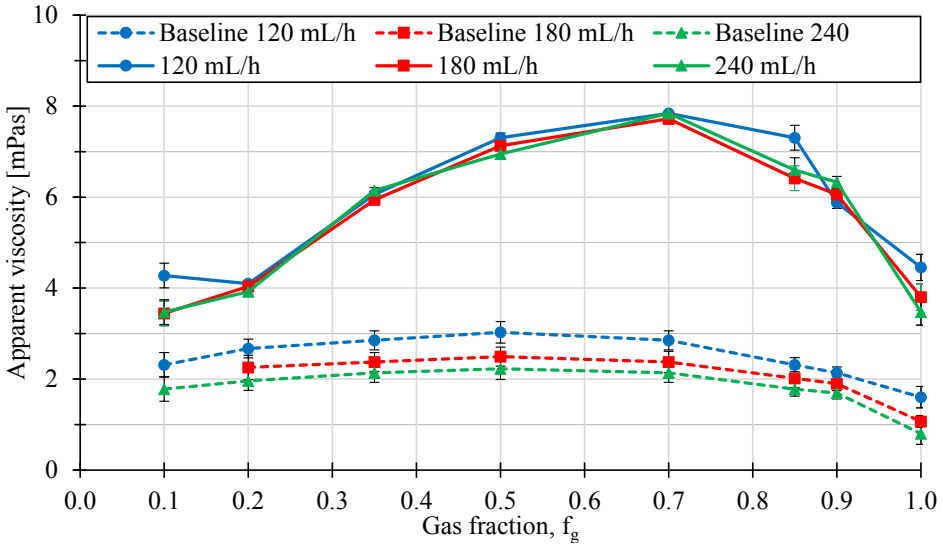

Figure 20: Apparent viscosity as a function of gas fraction during drainage-like co-injection of CO_2 and NanofluidA (solid lines) in Bentheimer sandstone. Co-injections with NPA were benchmarked against baseline co-injections with CO_2 and brine (dashed lines) at identical conditions.

Hysteresis effects on foam behavior were evaluated by comparing drainage-like (Figure 20) and imbibition-like apparent viscosities (Figure 21). A significant hysteretic effect related to gas fractional flow sequence indicated that foam strength is dependent on the history of the saturation change, i.e. previous injections conducted in the core plug [106]. This observation is important when obtaining input to simulation models. The application of foam scans for injection strategies in field are discussed in Sections 1.6.3 and 2.1.3, where the highest apparent viscosity measured is used to determine injection slug size ratios and as input in simulation models (*e.g.* fmmob, Equation 10). This finding influenced the decision of performing foam scans on 100% water saturated core plugs when collecting data for the field-pilot simulation model

(Figure 11).

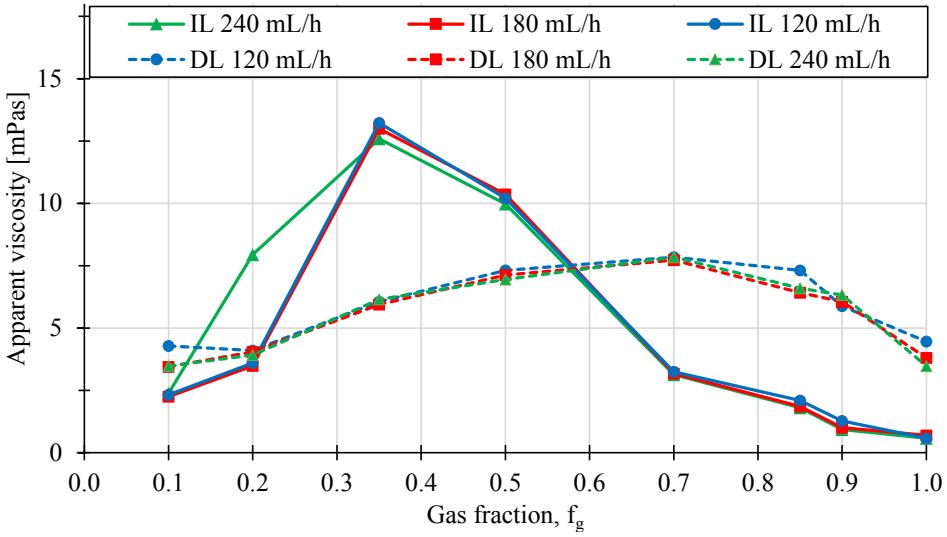

Figure 21: Hysteresis effect during foam scans at different injection rates in Bentheimer sandstone. Foam behavior differs significantly during imbibition-like injection sequence (dotted lines, IL) and drainage-like injection sequence (solid lines, DL). Optimal apparent viscosities were 7.8 mPas for drainage-like injection sequence (at f_g=0.70) and 14.2 mPas for imbibition-like injection sequence (at f_g=0.35). Near-Newtonian foam behavior was observed for both injection sequences.

By measuring the gas saturation in the core plug during a full injection cycle (drainage-like followed by imbibition-like) a significant difference in gas saturation was found (Figure 21). This suggests that gas saturation contributes to some of the reduction in flow potential for the core plug, but no consistent correlation between gas saturation and apparent viscosity was found. Hence, hysteresis from gas saturation cannot explain the total observed discrepancy. Although trapped gas (immobile gas due to foam generation and stationary liquid films) reduces gas flow relative to flowing gas and has previously been reported to significantly influence gas mobility [107], this cannot be measured directly in these experiments.

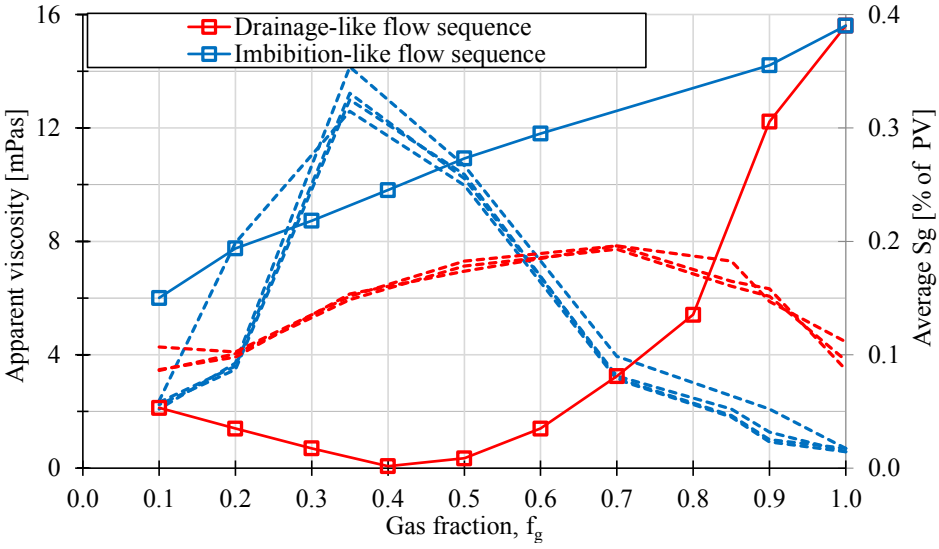

Figure 22: Apparent viscosity (dashed lines, primary vertical axis) and average gas saturation (solid lines, secondary vertical axis) as a function of gas fraction for a full cycle injection sequence (drainage-like: red, imbibition-like: blue). Increased gas saturation difference is observed during increasing apparent viscosity of imbibition-like injection sequence.

Effect of foaming agent

For comparison, a surfactant-stabilized CO_2-foam was evaluated under the same experimental conditions (AOS surfactant, Figure 23). Results showed a significant increase in foam strength, with a maximum apparent viscosity over two orders of magnitude higher than nanoparticle-stabilized foams (1.70 Pas at 120 mL/h and 0.88 Pas at 240 mL/h). Optimal gas fraction was achieved at $f_g = 0.90$ and the foam displayed shear-thinning behavior following from increased injection rate (120 mL/h to 240 mL/h). Results indicate higher foam generation from surfactants, and a reduced ability to stabilize foams at increased injection rates (shear-thinning). Nanoparticle-stabilized foams are more resilient to rate increase.

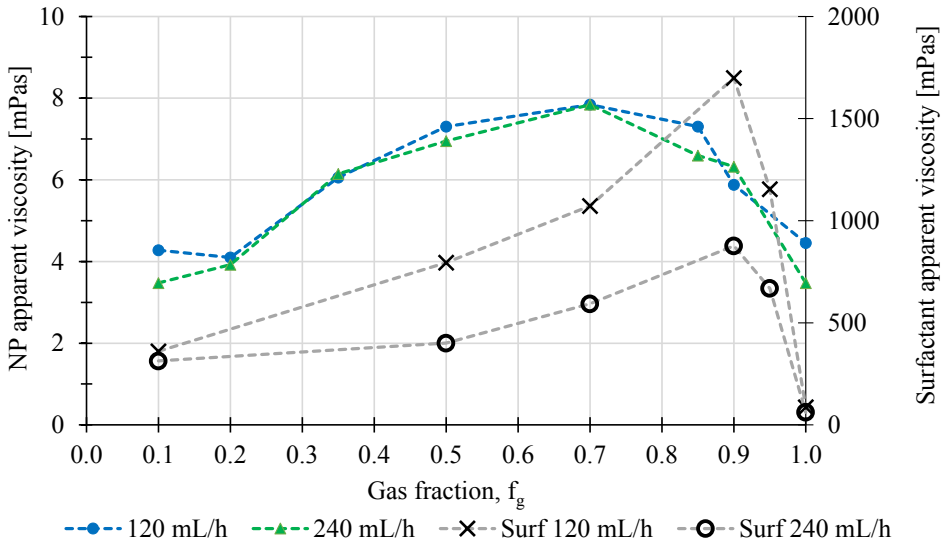

Figure 23: Comparison of foam strength (apparent viscosity) with nanoparticle-stabilized CO_2-foams (blue and green lines, primary vertical axis) and surfactant-stabilized CO_2-foams (gray lines, secondary vertical axis) as a function of gas fraction and injection rate. All injections followed a drainage-like injection sequence, and were performed in sandstone at the same experimental conditions.

Foam performance for EOR depends largely on the ability of the foaming agent to remain stable in the presence of oil [64]. To further evaluate the potential of nanoparticles as foam stabilizing agents, several foam injections were performed in crude oil saturated sandstone core plugs (Paper 5). The effects of nanoparticle concentration and degree of hydrophilicity (NPA vs. NPB) were examined and compared to foam performance of surfactant-stabilized foams at the same conditions. Emphasis was put on increasing the statistical significance of reported results. Several sets of experiments were performed (three or four) and oil production was measured at every 0.1 PV injected to facilitate statistical analysis of recovery profiles. Reported results are given with uncertainties as standard error from the mean for all sets of experiments (N>1) and as measurement uncertainty for single injection tests. The temperature was increased from 20ºC (foam scans) to 60ºC, pore pressures were kept at 90 bar and SurfA was used.

Baseline co-injections produced 8.2 ± 2.2 %* (%* = percentage-points) incremental oil (measured during tertiary EOR after waterflood), and the pressure gradient increased

with 39 ± 4% (ratio of pressure gradient at the end of co-injection to pressure gradient at the end of waterflood). By comparing the increase in pressure gradient to incremental oil recoveries for several sets of co-injections, three main observations were made (Figure 24). Firstly, all co-injections with NPA and NPB show a positive correlation between incremental oil recovery and pressure gradient increase compared to baseline injections. This suggests that nanoparticles generate and stabilize CO_2-foams in presence of crude oil, yielding a higher recovery factor. NPA increased the pressure gradient by a factor of 3 and recovered 71 ± 29% more oil compared to baseline co-injection (baseline 8.2% of OOIP; NPA 14.1% of OOIP). The observed effect of increasing the nanoparticle concentration from 1500 mPPM to 5000 mPPM was insignificant with respect to oil production (1.3 %* OOIP increase), but the foam stabilizing effect was larger (191 ± 39% increase in pressure gradient, a factor 5 higher than baseline). Secondly, NPB (less hydrophilic) improved oil recovery and foam strength to a much smaller degree compared to NPA. For hydrophilic particles, a lower degree of hydrophilicity increases adsorption energies on interfaces (Equation 8, Section 1.4.2) which seems to adversely affect foam performance. This might relate to the ratio of nanoparticles located at the interface between brine and CO_2, which is expected to be lower for less hydrophilic particles because of the energy required to move from bulk to the interface. And lastly, SurfA greatly improved the oil recovery (15.9 ± 1.4% of OOIP), whereas the pressure gradient decreased during co-injection (-13 ± 6%). This shows that the EOR mechanism for surfactant floods is different from that of nanoparticle floods. For these experiments, the increased oil recovery during co-injection with surfactant solution is likely dominated by an IFT reduction and associated capillary number increase (Equation 6, Section 1.4.2 and Figure 17), as no foam generation was observed. Surfactants showed high ability to generate foam in pore- and core-scale co-injections without oil (Papers 2, 3 and 4), but experienced a significant reduction in foam-stabilizing ability when crude oil was present. Nanoparticle-stabilized foams demonstrated a positive correlation between foam strength and incremental oil recovery for all injection tests. Other studies have also shown that nanoparticle-stabilized foams are stable in the presence of oil [108-110]. Foam formation is therefore likely the main EOR mechanism, with contributions from

reduced IFT (lesser for nanoparticles, compared to SurfA, according to Figure 17) between water and oil.

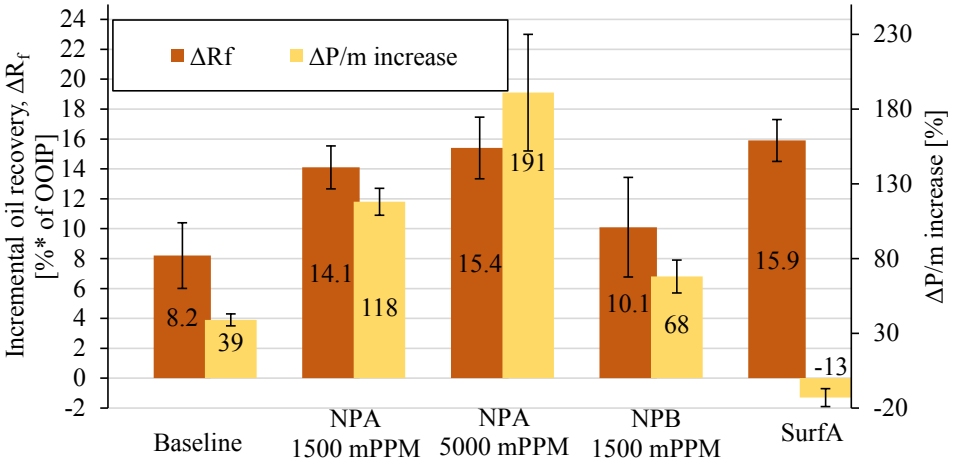

Figure 24: Incremental oil recovery (brown, primary vertical axis) and corresponding pressure gradient increase (yellow, secondary vertical axis) during co-injection of supercritical CO_2, brine (baseline) and three different foaming agents (NPA, NPB and SurfA).

2.2.4 Meta-Analysis of CO_2-Foams by Nanoparticles

Establishing cause and effect from multi-phase fluid flow in porous media relies on high experimental accuracy and low influence of underlying variables. A meta-analysis of all nanoparticle-stabilized CO_2-foam injections included in this dissertation was performed to evaluate the cause and effect between nanoparticle-stabilized foams (foam strength) to EOR and CO_2 storage. In total, 25 co-injections were evaluated based on their pressure gradient increase (used as a proxy for foam strength), incremental oil recovery and CO_2 storage, categorized into 10 groups based on experimental conditions (Table 2). All injections were performed at 90 bar pore pressures, constant $f_g = 0.70$, with NPA (except group D) at 60ºC (except groups B3, F and G) and with a nanoparticle concentration of 1500 mPPM (except C and G).

Table 2: Average values for parameters used to determine foam performance from nanoparticle stabilization. Each experiment is categorized with respect to experimental conditions, as shown in the first column (test group). Test groups B1, B2 and B3 are baseline co-injections and test groups A-G are nanoparticle-stabilized co-injections (compared to their respective baseline indicated in parenthesis). The number of experiments in each group are given by N, and all parameters are calculated as the difference between (end of) waterflood and (end of) co-injection during tertiary injection mode (Tert.) or difference between (end of) co-injection and initial conditions during secondary injection mode (Sec.).

Test group	Inj. Mode	N	ΔS_o [%PV]	ΔS_w [%PV]	CO_2 stored [%PV]	ΔR_f [%OOIP]	VEE	$\Delta P/m$ increase [%]
B1	Sec.	2	39	25	14	59	0.4	NA
B2	Tert.	4	6	6	11	8	2.0	39
B3	Tert.	1	3	2	5	4	1.7	27
A (B1)	Sec.	2	50	24	27	75	0.5	NA
B (B2)	Tert.	4	11	13	24	14	2.3	118
C (B2)	Tert.	4	10	3	14	15	1.3	191
D (B2)	Tert.	2	7	12	19	10	2.8	68
E (B2)	Tert.	1	9	5	14	12	1.5	97
F (B3)	Tert.	3	10	12	22	14	2.2	108
G (B3)	Tert.	2	7	15	22	10	3.2	102

The results from the meta-analysis show that nanoparticle-stabilized CO_2-foams increased: i) CO_2 storage by 137 ± 46%; ii) oil recovery by 91 ± 27%; and iii) pressure gradient by 213 ± 39%. Foam strength (measured as increase in pressure gradient) and its effect on oil recovery and CO_2 storage displays a strong positive correlation (Figure 25), with correlation coefficients, *r*, of 0.88 and 0.81 for ΔR_f vs. $\Delta P/m$ increase and CO_2 stored vs. $\Delta P/m$ increase, respectively. This correlation and the observed fluid diversion from foam generation on pore-scale (Section 2.1.2) suggest that foam mechanisms at field-scale (increased sweep and oil recovery from foam generation) are displayed in laboratory scale experiments.

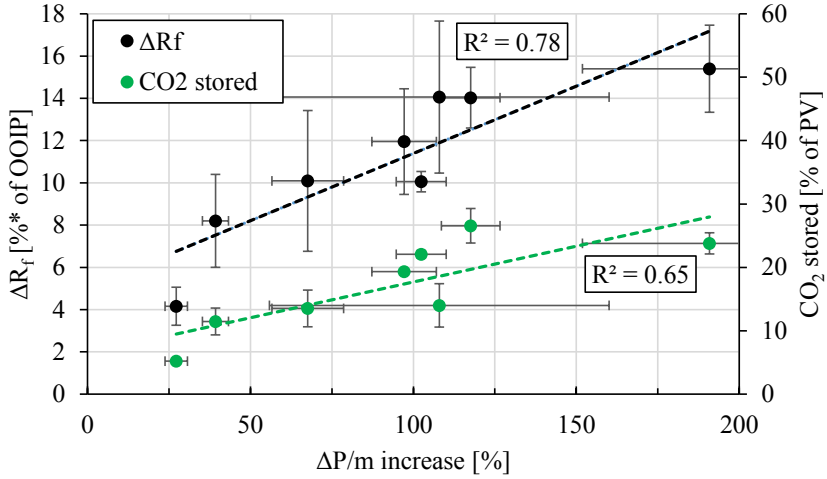

Figure 25: Incremental oil recovery (black, primary vertical axis) and CO_2 storage (green, secondary vertical axis) as a function of increased pressure gradient for 25 EOR injections in sandstone. Average values (if N>1) are calculated for 10 different groups (solid dots), categorized with respect to initial conditions. A strong positive linear correlation (dotted lines) is observed with a correlation coefficient of 0.88 and 0.81, for ΔR_f and CO_2 stored vs. $\Delta P/m$ increase, respectively.

2.3 CO_2 Storage for Carbon Negative Oil Production

For field-scale implementation of CO_2 injection for EOR, an accurate account of CO_2 usage is important [111]. CO_2 used is often represented as the amount of CO_2 required to produce one barrel of oil, quantified as the CO_2 utilization factor, UF_{CO2} [112]. The total CO_2 storage is a combination of porous media properties (heterogeneity, wettability, permeability and porosity) and operational parameters (well pattern, inter-well distance and injection strategies). For these reasons it is challenging to predict CO_2 use during EOR. Poor sweep efficiency and early CO_2 breakthrough cause high recycling rates and increased operational costs.

Using CO_2-foam for EOR in a CCUS context implies focus on the added-value from CO_2-foam (incremental oil recovery) and the CO_2 storage during this process. In this work CO_2 storage was evaluated during secondary and tertiary foam injections. Conservation of mass combined with volumetric flux from injection and production parameters were used to calculate the amount of CO_2 stored from change in (average) gas saturation in the core plugs. Correlations between foam strength (increase in pressure gradient), EOR (incremental oil recovery) and CO_2 storage (S_g after EOR), enabled quantification of carbon intensity from a CO_2-foam process to be determined. A laboratory analog to UF_{CO2}, volume element exchange (VEE), was implemented for core-scale experiments. VEE is defined as the ratio of volume elements of CO_2 stored to the volume elements of oil recovered during tertiary EOR at experimental conditions. VEE relates to the efficiency of the CCUS process by including the effect of CO_2 injection and CO_2-foam injection on water and oil displacement.

CCUS analysis on nanoparticle-stabilized foams (NPA) at tough conditions (high salinity and temperature, Paper 6) shows that (Figure 26): i) the pressure gradients increased with ~150-300% (high salinity: 147%; 1500 mPPM: 296%; 5000 mPPM: 276%); ii) the incremental oil recoveries increased with ~50-250% (high salinity: 46%; 1500 mPPM: 238%; 5000 mPPM: 142%); and iii) CO_2 storage increased with ~20-320% (high salinity: 22%; 1500 mPPM: 324%; 5000 mPPM: 324%). Observations suggest that nanoparticle-stabilized foam performance improves at higher temperatures

(and constant brine salinity) and reduces with increasing brine salinity, compared to results obtained at lower temperatures and salinities (Figure 24).

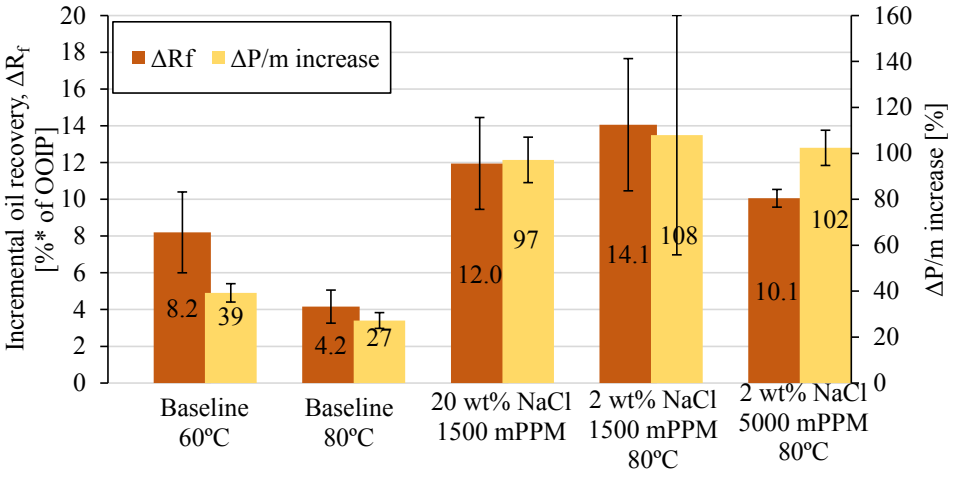

Figure 26: Incremental oil recovery (brown, primary vertical axis) and corresponding pressure gradient increase (yellow, secondary vertical axis) during co-injection of supercritical CO_2 and brine (baseline) at 60ºC and 80ºC, and NPA-stabilized foams at harsh conditions (20 wt% NaCl or 80ºC). Foam stabilization is observed, with a positive correlation between increase in pressure gradient (ratio of pressure gradient at end of co-injection to pressure gradient at end of WF) and incremental oil recovery.

VEE calculations from these experiments showed that the introduction of a third phase (CO_2) reduced the saturation of the two other phases (oil and water) and that incremental oil recovery correlated positively with increased water displacement (Figure 27). This is an important aspect of CO_2-foam flooding in a CCUS context; CO_2 mobility reduction by foam enables higher CO_2 storage by mobilizing oil and water in comparison to floodings without foam. This means that the volume (pore space) available for CO_2 storage increases more than what is expected from oil displacement alone.

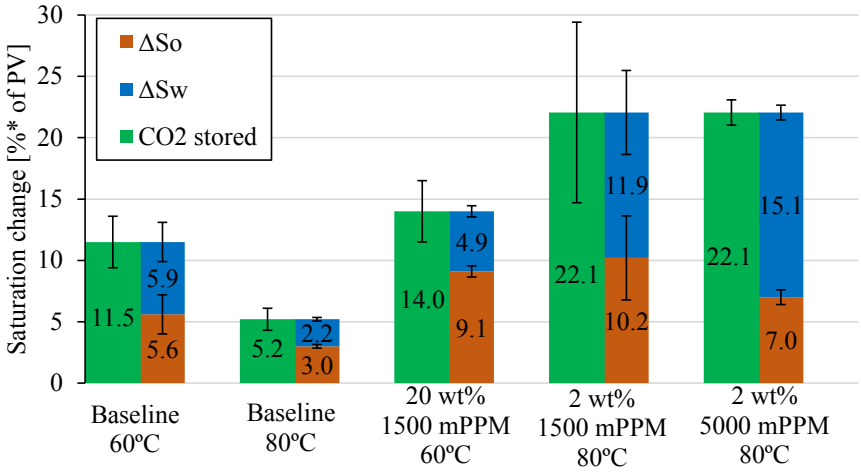

Figure 27: CO_2 storage (green), reduction in water saturation (blue) and reduction in oil saturation (brown) during tertiary CO_2-foam EOR core floods. Nanoparticle-stabilized foams increase CO_2 storage during EOR by increasing both oil and water displacement compared to co-injections without foam.

Since CO_2 is stored *ex-ante* (before the oil is produced and combusted), the carbon footprint from the EOR production can be expressed as (not including other emissions) the ratio of molecules of CO_2 stored to molecules of CO_2 released during oil combustion (equivalent to the ratio of C-atoms stored to C-atoms produced). If this ratio is one the oil displacement process is carbon neutral, meaning that the amount of CO_2 released from oil combustion is equal to the amount of CO_2 stored during EOR. Carbon negative oil displacement is achieved if the ratio is larger than one (more CO_2 molecules are stored during oil recovery than are produced from the combustion of the recovered oil). Molecules of CO_2 stored can be calculated directly from CO_2 volumes stored and CO_2 density at experimental conditions. The produced crude oil composition was not analyzed for molecular content in this dissertation, but is expected to vary with injection time and experimental conditions (Paper 1, Section 2.1.1). In a CCUS context, the EOR by CO_2 can be evaluated based on the carbon footprint, quantified in terms of degree of carbon neutrality (C-atoms stored to C-atoms produced). Mineral oil saturated core plugs (*n*-Decane, 10 C-atoms per molecule) were used to evaluate the degree of C-neutrality during CO_2-foam injections for EOR (Figure 28). Outcrop rock of sandstone and limestone were used under different experimental conditions.

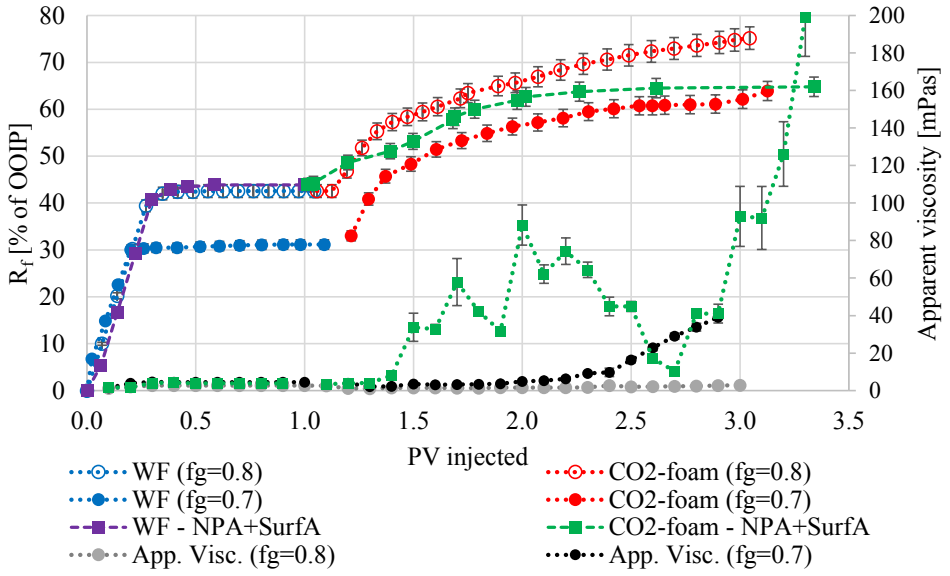

Figure 28: Recovery factor (primary vertical axis) and apparent viscosity (secondary vertical axis) as a function of PV injected during secondary waterflood and tertiary CO_2-foam flood. Blue and red curves: injections with SurfA (1 wt%) as foaming agent and gas fractions of f_g = 0.70 and f_g = 0.80, performed at 179 bar pore pressures and 60ºC in limestone (ES field analogue). Purple and green curve: co-injections with f_g = 0.70 using a combination of NPA (0.15 wt%) and SurfA (0.5 wt%), performed at 140 bar and 40ºC in sandstone. Observations showed improved foam strength with decreased gas fraction and that a strong foam is generated by combining nanoparticles and surfactants.

Converting VEE to molecular exchange demonstrates that a carbon neutral oil recovery was obtained for SurfA with f_g = 0.70, where 96 ± 7% of the produced C-atoms were stored. The carbon footprint from the EOR process using NPA and SurfA as foaming agents was negative (Figure 29), storing 142 ± 8% of the C-atoms that would be released during combustion of the incremental oil recovered. The presented foam injection combining NPA and SurfA has not yet been published in a journal and was selected from several injection tests to display the potential from combining surfactants and nanoparticles. Favorable synergies from using mixtures of nanoparticles and surfactants have recently been reported for nitrogen- and CO_2-foams [13, 108, 113, 114].

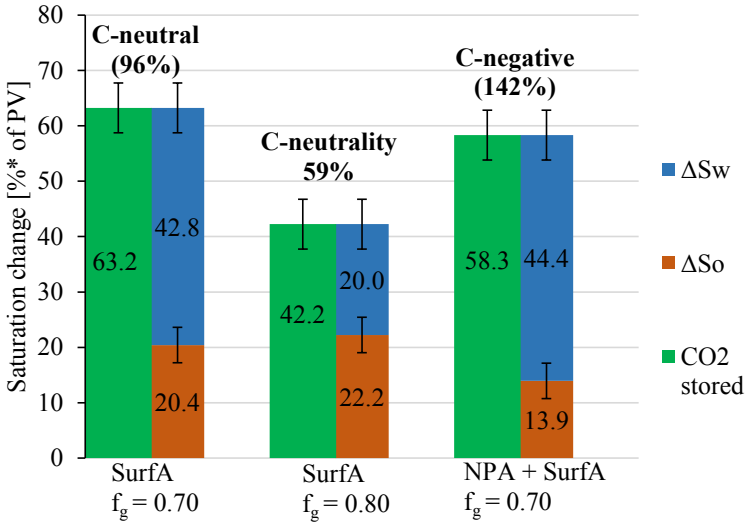

Figure 29: CO_2 storage (green), reduction in water saturation (blue) and reduction in oil saturation (brown) during tertiary CO_2-foam EOR core floods. SurfA-stabilized foams increased CO_2 storage during EOR from a 10 percentage-point reduction in gas fraction ($f_g = 0.80$ to $f_g = 0.70$) which results in a carbon neutral oil production process (96% of released C-atoms were stored). Combining SurfA and NPA generated a strong foam, resulting in a carbon neutral oil production process that yielded a storage of 142 ± 8% of the produced C-atoms.

Comparisons made between nanoparticle- and surfactant-stabilized foams in this work (Sections 2.2.2 and 2.2.3) indicate that surfactants have a higher ability to generate foams (pore-scale: foam texture, core-scale: apparent viscosity), while nanoparticles display a greater potential to stabilize foams (pore-scale: apparent viscosity with oil and Near-Newtonian flow behavior). This might in part be related to higher IFT reduction by surfactants (reduced energy requirement for foam generation, Equation 7) and greater interface adsorption energies by nanoparticles (Equation 8). Surfactant-stabilized foams display shear-thinning behavior, while nanoparticle-stabilized foams demonstrated no adverse effect from higher injection rates. A mixture of surfactants and nanoparticles, therefore, might prove beneficial in a CCUS context from increased foam generation (in zones with low oil saturation, surfactant effect) and enhanced foam stability (for high flow zones and zones with higher oil saturation, nanoparticle effect).

3. Conclusions

A key element in this dissertation has been the use of a bottom-up approach to evaluate CO_2-foam behavior in porous media. Co-injections in high-pressure micromodels enabled direct pore-scale evaluation of foaming agent performance with respect to foam texture, foam stability and flow diversion. More realistic reservoir conditions were gradually introduced through changing: i) system size (pore-to-core); ii) temperature (room temperature to reservoir temperatures); iii) salinity (salt concentration and ionic strength); and iv) oil phase (mineral and crude oils); and v) rock material (outcrop material with low heterogeneity and reservoir material with high heterogeneity). Emphasis was put on representing results with a high degree of accuracy, facilitated through statistical analyses on repeated experiments administered at the same conditions. The results show that CO_2-foams reduce gas mobility and have a great potential for use in a CCUS context by increasing oil recovery and CO_2 storage.

3.1 CO_2-Foam from Lab-to-Field

A CO_2-foam system was evaluated and optimized for implementation in a heterogeneous carbonate field in the US. The main findings were:

- CO_2 enables fluid transport through tight shale oil core plugs, resulting in oil production. Unstable displacement fronts adversely affected oil recovery by early CO_2 breakthrough and low sweep efficiency.
- The pre-selected field-specific surfactant (SurfA) generated strong CO_2-foams during co-injections in micromodels at high pressures. Bubble concentration was over two orders of magnitude higher compared to baseline co-injections. The stabilization effect was evaluated by foam half-life calculations at static conditions, with a calculated half-life of 13.3 ± 4.0 hours and a normalized bubble concentration of 37% after 72 hours.
- Field slug size ratio of CO_2 to brine was determined to be 0.70 based on results from foam quality scans in reservoir core plugs. Laboratory injections showed high CO_2 mobility reduction, with a MRF of 25 at $f_g = 0.70$.

- Surfactant concentration in brine slug (C_{surf} = 0.5 wt%) was selected based on foam strength measured from foam quality scans with reservoir crude oil (~S_{or}) and tertiary CO_2-foam EOR in reservoir core plugs.
- Field-scale simulations with laboratory derived input data (relative permeability curves from un-steady state CO_2/water displacements, f_g = 0.70 and C_{surf} = 0.5 wt%) demonstrated favorable foam performance from improved CO_2 utilization and reduced GOR, when comparing SAG- to WAG-injections.

3.2 Nanoparticles for CO_2-Foam

The application of hydrophilic silica nanoparticles as foaming agents was studied through a series of tests on core- and pore-scale. The main findings were:

- NPA was stable in brines with salinities up to 20 wt% NaCl and 5 wt% $CaCl_2$, and flowed unrestricted through sandstone cores with low retention (0.40 mg/g at 20ºC and 0.53 mg/g at 120ºC).
- Insignificant CO_2-foam generation was demonstrated during pore-scale observations of NPA and CO_2 at 90 bar pore pressure. At core-scale, NPA stabilized CO_2-foams during co-injections without oil, obtaining a foam with maximum apparent viscosity of 7.8 mPas at f_g = 0.70 (MRF = 3.8). Near-Newtonian flow behavior from increased injection rate was observed.
- Surfactant-stabilized CO_2-foams were over two orders of magnitude stronger than nanoparticle-stabilized foams with a maximum apparent viscosity at f_g = 0.90 in the absence of oil. Shear-thinning flow behavior from increased injection rate was observed.
- Nanoparticles displayed stabilizing effects in the presence of crude oil for all co-injections of nanofluid and CO_2, while surfactant-stabilized foams collapsed. Incremental oil recovery was similar for nanoparticle-stabilized foams and co-injections of surfactant solution and CO_2.
- A meta-analysis of nanoparticle-stabilized CO_2-foam injections (18 individual injections, categorized into 7 groups) shows an increased: i) pressure gradient

of 213 ± 39%; ii) oil recovery by 91 ± 27%; and iii) CO_2 storage of 137 ± 46% compared to baseline (7 individual injections, categorized in 3 groups).

- Combining NPA and SurfA generated the strongest foam observed during tertiary co-injections, with an apparent viscosity of 199 ± 21 mPas at S_{or} of ~0.25. The combined foam stabilizing effect of nanoparticles and surfactant resulted in an incremental oil recovery of 21 ± 2% of OOIP and a carbon negative oil production.

3.3 CO_2 Storage

Quantifying CO_2 storage potential and use are essential aspects of an EOR for CCUS process. CO_2 storage was evaluated during tertiary CO_2-foam injections and the key findings were:

- A meta-analysis of all nanoparticle-stabilized CO_2-foam injections included in this dissertation (18 individual injections, categorized into 7 groups) shows an increased CO_2 storage of 137 ± 46% compared to baseline co-injections (7 individual injections, categorized into 3 groups).
- In tertiary injection mode (N=16), the nanoparticle-stabilized CO_2-foams increase oil displacement (104 ± 26%), water displacement (201 ± 88%), CO_2 stored (144 ± 49%) and the pressure gradient (230 ± 42%) compared to baseline injections (N=5).
- Carbon neutral oil displacement was observed for CO_2-foam injection with SurfA in an outcrop limestone core plug with a 96 ± 7% *ex-ante* storage of produced C-atoms. For a foam injection with a combination of NPA and SurfA in sandstone, carbon negative oil production was observed storing 142 ± 7% of the produced C-atoms.

4. Future Perspectives

This dissertation demonstrates the potential benefits of using CO_2-foams for EOR. In a CCUS context, CO_2-foam implementation reduces the carbon footprint from the oil production process and has demonstrated carbon negative oil displacement. To obtain a significant reduction in CO_2 emissions while continuing to supply the world with cheap, plentiful and reliable energy, large-scale implementation of optimized foam systems in mature reservoirs is a promising technology. Optimizing foam systems requires a deep understanding of all aspects related to foam flow in porous media. Future extensions on the experimental work presented in this dissertation should put emphasis on foam performance in less water-wet core material in the presence of oil. Micromodels can be used to study the effect of different foaming agents on foam performance. Implementing a software capable of detecting interfaces for statistical representation of obtained empirical data would allow for inherent micromodel properties such as pore size distribution, aspect ratio and correlation number to be evaluated in relation to foam texture (bubble sizes, shapes and distributions), foam generation mechanisms and foam stabilization mechanisms. In addition, foam generation mechanisms could be determined from interface analyses during foam floods at lower injection rates or by implementing a camera with shorter shutter speed *i.e.* that takes more pictures per unit time. Foam quality scans should be performed with continuous oil injection, since it enables foam strength to be determined as a function of oil saturation.

A promising, cost efficient way of obtaining high performing field-specific foam systems could be found in the synergies that arise from using nanoparticles and surfactants as foaming agents. Research has shown that combinations increase [45, 114, 115] and reduce [116, 117] overall performance. The interplay between nanoparticles and surfactants must therefore be evaluated. The work presented in this dissertation suggests that surfactants are better foam generators, while nanoparticles are better foam stabilizers. Combining these effects should generate foams with a high lamella concentration (surfactant effect), producing large surface areas for nanoparticles to adsorb onto and stabilize.

4.1 Field Pilot Project

Laboratory investigations show that surfactant-stabilized CO_2-foam reduces gas mobility, increases oil recovery and diverts fluid flow. Obtained input parameters for the numerical simulator enabled predictions of field-scale foam performance through core-to-field up-scaling. Verifying foam performance at field-scale is an important extension of the work presented in this dissertation. Data collection and monitoring before, during and after SAG injection should include:

- Inter-well tracer tests to determine CO_2 breakthrough time
- Single-well tracer tests to estimate remaining oil saturation
- 4D seismic surveys to quantify CO_2 storage and mobility control through CO_2 saturation distribution
- Fall-off pressure tests to determine injection interval
- Reservoir zone specific injection profiles to determine fluid flow in different zones and verify flow diversion from foam

A continuous evaluation and implementation of the obtained data will contribute towards a better understanding of foam behavior at field-scale and improve future performance predictions from simulations.

Abbreviations

A	area
AOS	alpha-olefin sulfonate
CCS	carbon capture and storage
CCUS	carbon capture, utilization and storage
UF_{CO2}	CO_2 utilization factor
DL	drainage-like injection sequence
ES	East Seminole
EOR	enhanced oil recovery
e.g.	*exempli gratia,*"for example"
GOR	gas oil ratio
GHG	greenhouse gas
i.e.	*id est,* "in other words"
IL	imbibition-like injection sequence
IFT	interfacial tension
IPCC	Intergovernmental Panel on Climate Change
L	length
LE	local equilibrium
MRF	mobility reduction factor
FM	modeling mobility reduction factor
NPA	nanoparticle A (hydrophilic)
NPB	nanoparticle B (less hydrophilic)
NA	not applicable
OOIP	original oil in place
PB	population balance
PV	pore volume
Sec.	secondary injection mode
SD	standard deviation
SE	standard error
SurfA	surfactant A, Surfonic L24-22 (ES field specific)
SAG	surfactant alternating gas
T	temperature
Tert.	tertiary injection mode
UiB	University of Bergen
WAG	water alternating gas
WF	waterflooding

Nomenclature

N	number of repeated experiments in a specific category
%*	percentage-points
˚C	degrees Celsius
C_0	initial concentration
C_{out}	effluent concentration
C_{surf}	surfactant concentration
E	energy
E_D	microscopic displacement efficiency
E_R	recovery efficiency
E_v	macroscopic displacement efficiency
f_g	gas fraction
F_i	foam model functions
fmmob	reference mobility-reduction factor
k	absolute permeability
k_{eff}	effective permeability
k^f_{rg}	gas relative permeability without foam
k^{nf}_{rg}	gas relative permeability with foam
k_{rf}	foam relative permeability
mN/m	milliNewton/meter
mPPM	parts per million by mass
N_C	capillary number
R_f	recovery factor
S_g	gas saturation
S_o	oil saturation
S_{or}	residual oil saturation
S_w	water saturation
u_i	superficial velocity phase i
wt%	weight percent
ΔP	differential pressure
ΔP/m (∇P)	pressure gradient
θ	contact angle
λ	fluid mobility
μ	viscosity
μ_{app}	apparent viscosity
σ_{ij}	interfacial tension between phase i and j

Unit Conversions

1	mPas	=	1	cP	=	0.001 Pas
1	bar	=	100	kPa	=	14.5 psi
1	wt%	=	10 000	mPPM		
1	MPa	=	10	bar		
1	acre	=	4047	m^2		
1	foot	=	0.3048	m		
1	inch	=	2.54	cm		
1	mN/m	=	1	dyne/cm		

Bibliography

1. IEA, *World Energy Outlook 2017*. 2017, International Energy Agency.
2. IEA, *World Energy Outlook 2018*. 2018, International Energy Agency.
3. IPCC, *Climate Change 2014: Synthesis Report. Contribution of Working Groups I, II and III to the Fifth Assessment Report of the Intergovernmental Panel on Climate Change [Core Writing Team, R.K. Pachauri and L.A. Meyer (eds.)]*. 2014, IPCC: Geneva, Switzerland. p. 151.
4. IPCC, *Special Report on Carbon Dioxide Capture and Storage Prepared by Working Group III of the Intergovernmental Panel on Climate Change*, O.D. Bert Metz, Heleen de Coninck, Manuela Loos and Leo Meyer, Editor. 2005: Cambridge University Press, UK. p. pp 431.
5. Harrison, B. and G. Falcone, *Carbon capture and sequestration versus carbon capture utilisation and storage for enhanced oil recovery.* Acta Geotechnica, 2014. **9**(1): p. 29-38.
6. Chu, S. and A. Majumdar, *Opportunities and challenges for a sustainable energy future.* Nature, 2012. **488**: p. 294.
7. Jarrell, P.M. and R.T. Jones, *Practical aspects of CO2 flooding*. Henry L. Doherty series. Vol. vol. 22. 2002, Richardson, Tex: Henry L. Doherty Memorial Fund of AIME, Society of Petroleum Engineers.
8. Taber, J.J., F.D. Martin, and R.S. Seright, *EOR Screening Criteria Revisited - Part 1: Introduction to Screening Criteria and Enhanced Recovery Field Projects.* 1997.
9. Enick, R.M., et al., *Mobility and Conformance Control for CO2 EOR via Thickeners, Foams, and Gels -- A Literature Review of 40 Years of Research and Pilot Tests*. 2012, Society of Petroleum Engineers.
10. Newton, L.E., Jr. and R.A. McClay, *Corrosion and Operational Problems, CO2 Project, Sacroc Unit*, in *SPE Permian Basin Oil and Gas Recovery Conference*. 1977, Society of Petroleum Engineers: Midland, Texas. p. 12.
11. Moritis, G., *Future for EOR and IOR: New companies, infrastructure, projects reshape landscape for CO2 EOR in US.* Oil and Gas Journal, 2001. **99**(20).
12. Kootungal, L., *Worldwide EOR Survey.* Oil and Gas Journal, 2008. **106**(15): p. 45-60.
13. Singh, R. and K.K. Mohanty, *Foam flow in a layered, heterogeneous porous medium: A visualization study.* Fuel, 2017. **197**: p. 58-69.
14. Koottungal, L., *2014 worldwide EOR survey.* Oil & Gas Journal, 2014. **112**(4).
15. Fernø, M.A., et al., *Mobility control during CO2 EOR in fractured carbonates using foam: Laboratory evaluation and numerical simulations.* Journal of Petroleum Science and Engineering, 2015. **135**: p. 442-451.
16. Islam, M.R. and A. Chakma, *A New Recovery Technique for Heavy-Oil Reservoirs With Bottomwater.* 1992.
17. Brock, W.R. and L.A. Bryan, *Summary Results of CO2 EOR Field Tests, 1972-1987.* 1989, Society of Petroleum Engineers.
18. Lambert, M.R., et al., *Implementing CO2 Floods: No More Delays!*, in *Permian Basin Oil and Gas Recovery Conference*. 1996, Society of Petroleum Engineers: Midland, Texas.

19. Enick, R.M. and D.K. Olsen, *Mobility and Conformance Control for Carbon Dioxide Enhanced Oil Recovery (CO2-EOR) via Thickeners, Foams, and Gels – A Detailed Literature Review of 40 Years of Research*. 2012, National Energy Technology Laboratory. p. 267.
20. Sydansk, R.D. and L. Romero-Zeron, *Reservoir Conformance Improvement*. 2010, Richardson, UNITED STATES: Society of Petroleum Engineers.
21. Afzali, S., N. Rezaei, and S. Zendehboudi, *A comprehensive review on Enhanced Oil Recovery by Water Alternating Gas (WAG) injection.* Fuel, 2018. **227**: p. 218-246.
22. Al Hinai, N.M., et al., *Experimental Evaluations of Polymeric Solubility and Thickeners for Supercritical CO2 at High Temperatures for Enhanced Oil Recovery.* Energy & Fuels, 2018. **32**(2): p. 1600-1611.
23. Heller, J.P., et al., *Direct Thickeners for Mobility Control of CO2 Floods.* Society of Petroleum Engineers Journal, 1985. **25**(05): p. 679-686.
24. Lemmon, E.W., M.O. McLinden, and D.G. Friend, *Thermophysical Properties of Fluid Systems*, in *in NIST Chemistry WebBook, NIST Standard Reference Database Number 69, Eds. P.J. Linstrom and W.G. Mallard, National Institute of Standards and Technology, Gaithersburg MD, 20899*. 2018.
25. Schramm, L.L., *Foams : fundamentals and applications in the petroleum industry*. Advances in chemistry series. Vol. 242. 1994, Washington, DC: American Chemical Society.
26. Stevenson, P., *Foam engineering : fundamentals and applications*. 2012, Wiley: Chichester, West Sussex.
27. Schramm, L.L., *Surfactants : fundamentals and applications in the petroleum industry*. 2000, Cambridge: Cambridge University Press.
28. Li, R.F., et al., *Foam Mobility Control for Surfactant Enhanced Oil Recovery.* 2010.
29. Dickson, J.L., B.P. Binks, and K.P. Johnston, *Stabilization of Carbon Dioxide-in-Water Emulsions with Silica Nanoparticles.* Langmuir, 2004. **20**(19): p. 7976-7983.
30. Bennetzen, M.V. and K. Mogensen, *Novel Applications of Nanoparticles for Future Enhanced Oil Recovery*, in *International Petroleum Technology Conference*. 2014, International Petroleum Technology Conference: Kuala Lumpur, Malaysia.
31. Rio, E., et al., *Unusually stable liquid foams.* Advances in Colloid and Interface Science, 2014. **205**: p. 74-86.
32. Xue, Z., et al., *CO2-Soluble Ionic Surfactants and CO2 Foams for High-Temperature and High-Salinity Sandstone Reservoirs.* Energy & Fuels, 2015. **29**(9): p. 5750-5760.
33. Zitha, P.L.J., et al., *Coupling of Foam Drainage and Viscous Fingering in Porous Media Revealed by X-ray Computed Tomography.* Transport in Porous Media, 2006. **64**(3): p. 301-313.
34. Kovscek, A.R. and C.J. Radke, *Fundamentals of Foam Transport in Porous Media*, in *Foams: Fundamentals and Applications in the Petroleum Industry*. 1994, American Chemical Society. p. 115-163.

35. Prud'homme, R.K. and S.A. Khan, *Foams : theory, measurements, and applications*. Surfactant science series. Vol. vol. 57. 1996, New York: Marcel Dekker.
36. Rossen, W.R., *Foams in Enhanced Oil Recovery*, in *Foams : theory, measurements, and applications*, R. Prud'homme and S. Khan, Editors. 1996, Marcel Dekker: New York.
37. Hirasaki, G.J. and J.B. Lawson, *Mechanisms of Foam Flow in Porous Media: Apparent Viscosity in Smooth Capillaries.* Society of Petroleum Engineers Journal, 1985. **25**(02): p. 176-190.
38. Schramm, L.L. and F. Wassmuth, *Foams: Basic Principles*, in *Foams: Fundamentals and Applications in the Petroleum Industry*. 1994, American Chemical Society. p. 3-45.
39. Henry, R.L., et al., *Field Test of Foam to Reduce CO2 Cycling*. 1996, Society of Petroleum Engineers.
40. Moffitt, P., et al., *East Vacuum Grayburg San Andres Unit, 30 Years of CO2 Flooding: Accomplishments, Challenges and Opportunities*. 2015, Society of Petroleum Engineers.
41. Chou, S.I., et al., *CO2 Foam Field Trial at North Ward-Estes*. 1992, Society of Petroleum Engineers.
42. Jonas, T.M., S.I. Chou, and S.L. Vasicek, *Evaluation of a C02 Foam Field Trial: Rangely Weber Sand Unit*. 1990, Society of Petroleum Engineers.
43. Hoefner, M.L., et al., *CO2 Foam: Results From Four Developmental Field Trials.* 1995.
44. Sanders, A., et al., *Implementation of a CO2 Foam Pilot Study in the SACROC Field: Performance Evaluation*. 2012, Society of Petroleum Engineers.
45. Yekeen, N., et al., *Bulk and bubble-scale experimental studies of influence of nanoparticles on foam stability.* Chinese Journal of Chemical Engineering, 2017. **25**(3): p. 347-357.
46. Holmberg, K., *Novel Surfactants: Preparation Applications And Biodegradability, Second Edition, Revised and Expanded*. 2003, New York Basel: Marcel Dekker, Inc.
47. Nguyen, Q., G. Hirasaki, and K. Johnston, *Novel CO2 Foam Concepts and Injection Schemes for Improving CO2 Sweep Efficiency in Sandstone and Carbonate Hydrocarbon Formations*. 2015, Univ. of Texas, Austin, TX (United States).
48. Jian, G., et al., *Static Adsorption of an Ethoxylated Nonionic Surfactant on Carbonate Minerals.* Langmuir, 2016. **32**(40): p. 10244-10252.
49. Simjoo, M., et al., *CT Scan Study of Immiscible Foam Flow in Porous Media for Enhancing Oil Recovery.* Industrial & Engineering Chemistry Research, 2013. **52**(18): p. 6221-6233.
50. Mannhardt, K., L.L. Schramm, and J.J. Novosad, *Effect of Rock Type and Brine Composition on Adsorption of Two Foam-Forming Surfactants.* SPE Advanced Technology Series, 1993. **1**(01): p. 212-218.
51. Mannhardt, K. and I. Svorstøl, *Surfactant concentration for foam formation and propagation in Snorre reservoir core.* Journal of Petroleum Science and Engineering, 2001. **30**(2): p. 105-119.

52. Zhang, X., et al., *A quasi-solid-state dye-sensitized solar cell based on the stable polymer-grafted nanoparticle composite electrolyte.* Journal of Power Sources, 2006. **160**(2): p. 1451-1455.
53. Wang, P., et al., *Enhance the Performance of Dye-Sensitized Solar Cells by Co-grafting Amphiphilic Sensitizer and Hexadecylmalonic Acid on TiO2 Nanocrystals.* The Journal of Physical Chemistry B, 2003. **107**(51): p. 14336-14341.
54. Briseno, A.L., et al., *Oligo- and Polythiophene/ZnO Hybrid Nanowire Solar Cells.* Nano Letters, 2010. **10**(1): p. 334-340.
55. Saunders, B.R. and M.L. Turner, *Nanoparticle–polymer photovoltaic cells.* Advances in Colloid and Interface Science, 2008. **138**(1): p. 1-23.
56. Medarova, Z., et al., *In vivo imaging of siRNA delivery and silencing in tumors.* Nat Med, 2007. **13**(3): p. 372-7.
57. Kumari, A., S.K. Yadav, and S.C. Yadav, *Biodegradable polymeric nanoparticles based drug delivery systems.* Colloids and Surfaces B: Biointerfaces, 2010. **75**(1): p. 1-18.
58. Auffan, M., et al., *Towards a definition of inorganic nanoparticles from an environmental, health and safety perspective.* Nat Nano, 2009. **4**(10): p. 634-641.
59. Binks, B.P., *Particles as surfactants—similarities and differences.* Current Opinion in Colloid & Interface Science, 2002. **7**(1–2): p. 21-41.
60. Falls, A.H., et al., *Development of a Mechanistic Foam Simulator: The Population Balance and Generation by Snap-Off.* SPE Reservoir Engineering, 1988. **3**(03): p. 884-892.
61. Falls, A.H., J.J. Musters, and J. Ratulowski, *The Apparent Viscosity of Foams in Homogeneous Bead Packs.* SPE Reservoir Engineering, 1989. **4**(02): p. 155-164.
62. Saint-Jalmes, A., *Physical chemistry in foam drainage and coarsening.* Soft Matter, 2006. **2**(10): p. 836-849.
63. Nguyen, Q.P., et al., *Experimental and Modeling Studies on Foam in Porous Media: A Review*, in *SPE International Symposium on Formation Damage Control*. 2000, Society of Petroleum Engineers: Lafayette, Louisiana. p. 22.
64. Farajzadeh, R., et al., *Foam–oil interaction in porous media: Implications for foam assisted enhanced oil recovery.* Advances in Colloid and Interface Science, 2012. **183-184**: p. 1-13.
65. Kahrobaei, S., S. Vincent-Bonnieu, and R. Farajzadeh, *Experimental Study of Hysteresis behavior of Foam Generation in Porous Media.* Scientific Reports, 2017. **7**(1): p. 8986.
66. Schramm, L.L., *Foam Sensitivity to Crude Oil in Porous Media*, in *Foams: Fundamentals and Applications in the Petroleum Industry*. 1994, American Chemical Society. p. 165-197.
67. Lake, L.W., *Fundamentals of enhanced oil recovery*. [2. utg.]. ed, ed. R.T. Johns, et al. 2014, Richardson, Tex: Society of Petroleum Engineers.
68. Simjoo, M. and P.L.J. Zitha, *Effects of Oil on Foam Generation and Propagation in Porous Media*, in *SPE Enhanced Oil Recovery Conference*. 2013, Society of Petroleum Engineers: Kuala Lumpur, Malaysia. p. 16.

69. Yeganeh, M., et al., *Capillary Desaturation Curve Fundamentals*, in *SPE Improved Oil Recovery Conference*. 2016, Society of Petroleum Engineers: Tulsa, Oklahoma, USA. p. 14.
70. Schramm, L.L. and S.M. Kutay, *Emulsions and Foams in the Petroleum Industry*, in *Surfactants: Fundamentals and Applications in the Petroleum Industry*, L.L. Schramm, Editor. 2000, Cambridge University Press: Cambridge. p. 79-118.
71. Sheng, J.J., *Chapter 7 - Surfactant Flooding*, in *Modern Chemical Enhanced Oil Recovery*, J.J. Sheng, Editor. 2011, Gulf Professional Publishing: Boston. p. 239-335.
72. Atkins, P.W., J. De Paula, and J. Keeler, *Atkins' physical chemistry*. Eleventh edition. ed. Physical chemistry. 2018, Oxford: Oxford University Press.
73. Alcorn, Z.P., *Upscaling CO2 foam for enhanced oil recovery and CO2 storage from laboratory to field scale : an integrated approach to designing a field pilot test*. 2018, University of Bergen: Bergen.
74. Alcorn, Z.P., et al. *CO2 Foam Field Pilot Test for EOR and CO2 Storage in a Heterogeneous Carbonate Reservoir: Operational Design, Data Collection and Pilot Monitoring Program*. in *80th EAGE Conference and Exhibition 2018* 2018. Denmark.
75. Kam, S.I., et al., *Dynamic Simulations With an Improved Model for Foam Generation.* SPE Journal, 2007. **12**(01): p. 35-48.
76. Kovscek, A.R., T.W. Patzek, and C.J. Radke, *A mechanistic population balance model for transient and steady-state foam flow in Boise sandstone.* Chemical Engineering Science, 1995. **50**(23): p. 3783-3799.
77. Kovscek, A.R., W.P. Tadeusz, and C.J. Radke, *Mechanistic Foam Flow Simulation in Heterogeneous and Multidimensional Porous Media.* SPE Journal, 1997. **2**(04): p. 511-526.
78. Kovscek, A.R., Q. Chen, and M. Gerritsen, *Modeling Foam Displacement With the Local-Equilibrium Approximation: Theory and Experimental Verification.* SPE Journal, 2010. **15**(01): p. 171-183.
79. Rossen, W.R., et al., *Simplified Mechanistic Simulation of Foam Processes in Porous Media.* SPE Journal, 1999. **4**(03): p. 279-287.
80. Schlumberger, *ECLIPSE Technical Description V2015.2*. 2015.
81. Ma, K., et al., *Modeling Techniques for Foam Flow in Porous Media.* SPE Journal, 2015. **20**(03): p. 453-470.
82. Ma, K., S.L. Biswal, and G.J. Hirasaki. *Experimental and Simulation Studies of Foam in Porous Media At Steady State*. in *AIChE Spring Meeting*. 2012. Houston, TX, 1-5 April.
83. Lotfollahi, M., et al., *Comparison of implicit-texture and population-balance foam models.* Journal of Natural Gas Science and Engineering, 2016. **31**: p. 184-197.
84. Darvish, G.R., et al., *Reservoir Conditions Laboratory Experiments of CO2 Injection into Fractured Cores*, in *SPE Europec/EAGE Annual Conference and Exhibition*. 2006, Society of Petroleum Engineers: Vienna, Austria. p. 15.
85. Busch, A., et al., *Carbon dioxide storage potential of shales.* International Journal of Greenhouse Gas Control, 2008. **2**(3): p. 297-308.

86. Eide, O., et al., *CO2 EOR by Diffusive Mixing in Fractured Reservoirs.* Petrophysics, 2015. **56**(01): p. 23-31.
87. Sheng, J.J., *Chapter 11 - Foams and Their Applications in Enhancing Oil Recovery*, in *Enhanced Oil Recovery Field Case Studies*, J.J. Sheng, Editor. 2013, Gulf Professional Publishing: Boston. p. 251-280.
88. Sheng, J.J., et al., *Experimental Study of Foamy Oil Stability.* Journal of Canadian Petroleum Technology, 1997. **36**(04): p. 8.
89. Simjoo, M., et al., *Foam stability in the presence of oil: Effect of surfactant concentration and oil type.* Colloids and Surfaces A: Physicochemical and Engineering Aspects, 2013. **438**: p. 148-158.
90. Alvarez, J.M., H.J. Rivas, and W.R. Rossen, *Unified Model for Steady-State Foam Behavior at High and Low Foam Qualities.* SPE Journal, 2001.
91. Osterloh, W.T. and M.J. Jante, Jr., *Effects of Gas and Liquid Velocity on Steady-State Foam Flow at High Temperature*, in *SPE/DOE Enhanced Oil Recovery Symposium*. 1992, Society of Petroleum Engineers: Tulsa, Oklahoma. p. 12.
92. Campbell, B.T. and F.M. Orr, Jr., *Flow Visualization for CO2/Crude-Oil Displacements.* Society of Petroleum Engineers Journal, 1985. **25**(05): p. 665-678.
93. Martin, D.F. and J.J. Taber, *Carbon Dioxide Flooding.* Journal of Petroleum Technology, 1992. **44**(04): p. 396-400.
94. Karakashev, S.I., et al., *Formation and stability of foams stabilized by fine particles with similar size, contact angle and different shapes.* Colloids and Surfaces A: Physicochemical and Engineering Aspects, 2011. **382**(1): p. 132-138.
95. Kim, I., et al., *Size-dependent properties of silica nanoparticles for Pickering stabilization of emulsions and foams.* Journal of Nanoparticle Research, 2016. **18**(4): p. 82.
96. Stocco, A., et al., *Aqueous foams stabilized solely by particles.* Soft Matter, 2011. **7**(4): p. 1260-1267.
97. Yang, W., T. Wang, and Z. Fan, *Highly Stable Foam Stabilized by Alumina Nanoparticles for EOR: Effects of Sodium Cumenesulfonate and Electrolyte Concentrations.* Energy & Fuels, 2017. **31**(9): p. 9016-9025.
98. Deleurence, R., C. Parneix, and C. Monteux, *Mixtures of latex particles and the surfactant of opposite charge used as interface stabilizers – influence of particle contact angle, zeta potential, flocculation and shear energy.* Soft Matter, 2014. **10**(36): p. 7088-7095.
99. Metin, C.O., et al., *Stability of aqueous silica nanoparticle dispersions.* Journal of Nanoparticle Research, 2011. **13**(2): p. 839-850.
100. Chang, H.G., *Factors affecting particle retention in porous media.* Emirates Journal for Engineering Research, 2007. **12**(3): p. 7.
101. Aadland, R., et al., *Identification of Nanocellulose Retention Characteristics in Porous Media.* Nanomaterials, 2018. **8**(7): p. 547.
102. Ju, B. and T. Fan, *Experimental study and mathematical model of nanoparticle transport in porous media.* Powder Technology, 2009. **192**(2): p. 195-202.

103. Yu, H., et al., *Transport and retention of aqueous dispersions of superparamagnetic nanoparticles in sandstone.* Journal of Petroleum Science and Engineering, 2014. **116**: p. 115-123.
104. Rodriguez Pin, E., et al., *Enhanced Migration of Surface-Treated Nanoparticles in Sedimentary Rocks*, in *SPE Annual Technical Conference and Exhibition*. 2009, Society of Petroleum Engineers: New Orleans, Louisiana. p. 21.
105. Schmitt, M., et al., *Classification and quantification of pore shapes in sandstone reservoir rocks with 3-D X-ray micro-computed tomography.* Solid Earth, 2016. **7**(1): p. 285-300.
106. Keelan, D.K. and V.J. Pugh, *Trapped-Gas Saturations in Carbonate Formations.* 1975.
107. Tang, G.-Q. and A.R. Kovscek, *Trapped Gas Fraction During Steady-State Foam Flow.* Transport in Porous Media, 2006. **65**(2): p. 287-307.
108. Singh, R. and K.K. Mohanty, *Synergy between Nanoparticles and Surfactants in Stabilizing Foams for Oil Recovery.* Energy & Fuels, 2015. **29**(2): p. 467-479.
109. Nguyen, P., H. Fadaei, and D. Sinton, *Pore-Scale Assessment of Nanoparticle-Stabilized CO2 Foam for Enhanced Oil Recovery.* Energy & Fuels, 2014. **28**(10): p. 6221-6227.
110. Yekeen, N., et al., *Experimental investigation of minimization in surfactant adsorption and improvement in surfactant-foam stability in presence of silicon dioxide and aluminum oxide nanoparticles.* Journal of Petroleum Science and Engineering, 2017. **159**: p. 115-134.
111. Azzolina, N.A., et al., *CO2 storage associated with CO2 enhanced oil recovery: A statistical analysis of historical operations.* International Journal of Greenhouse Gas Control, 2015. **37**: p. 384-397.
112. Peck, W.D., et al., *Best Practices for Quantifying the CO2 Storage Resource Estimates in CO2 Enhanced Oil Recovery.* Energy Procedia, 2017. **114**: p. 4741-4749.
113. Sun, Q., et al., *Utilization of Surfactant-Stabilized Foam for Enhanced Oil Recovery by Adding Nanoparticles.* Energy & Fuels, 2014. **28**(4): p. 2384-2394.
114. Li, S., Z. Li, and P. Wang, *Experimental Study of the Stabilization of CO2 Foam by Sodium Dodecyl Sulfate and Hydrophobic Nanoparticles.* Industrial & Engineering Chemistry Research, 2016. **55**(5): p. 1243-1253.
115. Guo, F. and S. Aryana, *An experimental investigation of nanoparticle-stabilized CO2 foam used in enhanced oil recovery.* Fuel, 2016. **186**: p. 430-442.
116. Kumar, S. and A. Mandal, *Investigation on stabilization of CO2 foam by ionic and nonionic surfactants in presence of different additives for application in enhanced oil recovery.* Applied Surface Science, 2017. **420**: p. 9-20.
117. Atkin, R., et al., *Mechanism of cationic surfactant adsorption at the solid–aqueous interface.* Advances in Colloid and Interface Science, 2003. **103**(3): p. 219-304.

Graphic design: Communication Division, UiB / Print: Skipnes Kommunikasjon AS

uib.no

ISBN: 978-82-308-3545-6